UPPSALA
UNIVERSITET

Digital Comprehensive Summaries of Uppsala Dissertations from the Faculty of Science and Technology 2168

Using Molecular Dynamics Simulations to Explore Critical Property Relationships in Polymer Electrolytes

Polarity, Coordination, Ionic transport, Ion-pairing, and Ion-ion Correlations

HARISH GUDLA

ACTA
UNIVERSITATIS
UPSALIENSIS
UPPSALA
2022

ISSN 1651-6214
ISBN 978-91-513-1555-3
URN urn:nbn:se:uu:diva-481109

Dissertation presented at Uppsala University to be publicly examined in Polhemssalen, Ångströmlaboratoriet, Lägerhyddsvägen 1, Uppsala, Friday, 23 September 2022 at 09:15 for the degree of Doctor of Philosophy. The examination will be conducted in English. Faculty examiner: Prof. Andreas Heuer (University of Münster).

Abstract
Gudla, H. 2022. Using Molecular Dynamics Simulations to Explore Critical Property Relationships in Polymer Electrolytes. Polarity, Coordination, Ionic transport, Ion-pairing, and Ion-ion Correlations. *Digital Comprehensive Summaries of Uppsala Dissertations from the Faculty of Science and Technology* 2168. 69 pp. Uppsala: Acta Universitatis Upsaliensis. ISBN 978-91-513-1555-3.

While ion transport in solid polymer electrolytes (SPEs) has been explored for decades, there still remains controversies about its fundamental properties, often correlated with gaps between experimental and computational studies. Using molecular dynamics simulations to understand the complex transport mechanisms and also to fill these gaps is the main goal of this thesis. This is achieved by critically examining the relationships between different properties in SPE systems: polarity, coordination, ion-pairing, and ion-ion correlations, which highly influence the ionic transport mechanism.

Firstly, the relation between polarity, ion-pairing, and ion-ion correlations was explored. The solvent polarity (ε_p) of poly(ethylene oxide) (PEO) doped with LiTFSI system is modulated using a charge scaling method. When separating the effects of solvent polarity and glass transition temperature, a maximum in the Li-ion diffusion coefficient with respect to ε_p is observed. This is attributed to the transitions in the transport mechanisms and an optimal solvating ability of Li-ion at intermediate values of ε_p. The solvent polarity also plays a critical role in the formation of charge-neutral ion pairs, which is commonly considered detrimental for ionic conductivity. The relation between cation−anion distinct conductivity and the lifetime of ion pairs was thereby examined, where it is found that short-lived ion pairs actually contribute positively to the ionic conductivity. Moreover, the origins of the recently observed negative transference numbers were scrutinized. A strong dependence of the reference frame in the estimation of the transference numbers is found, which explains observed differences between experiments and computations.

Secondly, the role of coordination chemistry and its influence on ion transport mechanisms and conduction properties in SPEs was studied. The change in the cation coordination with both polymers and anions was used to study the dominant transport mechanisms at different molecular weights and salt concentrations for PEO and a polyester-based SPE, which shows that essentially very little true hopping occurs in these materials. In this context, the coordination and ionic transport properties of three resemblant carbonyl-coordinating polymers are also investigated: polyketones, polyesters, and polycarbonates. The extra main-chain oxygens for the latter polymers are shown to decrease the electrostatic energy between Li-ion and the carbonyl group, and the cationic transference numbers are thus found to be increasing as the coordination strength decrease.

Keywords: Solid polymer electrolytes, molecular dynamics simulations, solvent polarity, ion-pairing, ion coordination, ion transport mechanisms

Harish Gudla, Department of Chemistry - Ångström, Structural Chemistry, Box 538, Uppsala University, SE-751 21 Uppsala, Sweden.

ISSN 1651-6214
ISBN 978-91-513-1555-3
URN urn:nbn:se:uu:diva-481109 (http://urn.kb.se/resolve?urn=urn:nbn:se:uu:diva-481109)

Dedicated to Athira, friends, and family.

List of Papers

This thesis is based on the following papers, which are referred to in the text by their Roman numerals.

I. **Gudla, H.**; Zhang, C.; Brandell, D. Effects of Solvent Polarity on Li-Ion Diffusion in Polymer Electrolytes: An All-Atom Molecular Dynamics Study with Charge Scaling. *J. Phys. Chem. B* **2020**, *124*, 8124–8131.

II. **Gudla, H.**; Shao, Y.; Phunnarungsi, S.; Brandell, D.; Zhang, C. Importance of the Ion-Pair Lifetime in Polymer Electrolytes. *J. Phys. Chem. Lett.* **2021**, *12*, 8460–8464.

III. Shao, Y.; **Gudla, H.**; Brandell, D.; Zhang, C. Transference Number in Polymer Electrolytes: Mind the Reference-Frame Gap. *J. Am. Chem. Soc.* **2022**., *144*, 7583–7587.

IV. **Gudla, H.**; Hockmann, A.; Brandell, D.; Mindemark, J. To Hop or Not to Hop – Unveiling Different Modes of Ion Transport in Solid Polymer Electrolytes Through Molecular Dynamics Simulations. *In manuscript*.

V. Eriksson, T.; **Gudla, H**.; Manabe, Y.; Yoneda, T.; Friesen, D.; Zhang, C.; Inokuma, Y.; Brandell, D.; Mindemark, J. Carbonyl-Containing Solid Polymer Electrolyte Host Materials: Conduction and Coordination in Polyketone, Polyester and Polycarbonate Systems. *Submitted manuscript.*

Reprints were made with permission from the respective publishers.

Disclaimer: Parts of this thesis are based on my licentiate thesis titled *Impact of Solvent Polarity on Ion Conduction and Ion-Pairing in PEO-LiTFSI: Atomistic Molecular Dynamics Studies* (Uppsala University, 2021)

Comments on my contributions to the appended papers:

For **Papers I**, **II**, and **IV**, I had the main responsibility for planning and performing simulations, analyzing the results, and writing the manuscripts. In **Paper III**, and **V**, I was mainly responsible for conducting the simulations, analyzing the results for the polymer electrolyte part, and writing the corresponding part of the manuscript.

Papers not included in the thesis:

VI. Unge, M.; **Gudla, H.**; Zhang, C.; Brandell, D. Electronic Conductivity of Polymer Electrolytes: Electronic Charge Transport Properties of LiTFSI-Doped PEO. *Phys. Chem. Chem. Phys.* **2020**, 1–9.

VII. Mai, C. T.; **Gudla, H.**; Edström, K.; Hernández, G.; Mindemark, J. The interfering effects of LiTFSI salt on the dimerization of UPy motifs in self-healing polymer electrolytes. *In manuscript*

Contents

Abbreviations

AIMD	*Ab-initio* molecular dynamics
BE	Binding energy
CIP	Contact ion-pairs
CN	Coordination number
DBP	Dynamic bond percolation
DFT	Density functional theory
FEM	Finite element methodology
GAFF	General AMBER force field
GK	Green-Kubo
kMC	kinetic Monte Carlo
LIB	Li-ion battery
MD	Molecular dynamics
MSCD	Mean squared cross displacement
MSD	Mean squared displacement
NE	Nernst-Einstein
PCL	Poly(ε-caprolactone)
PEO	Poly(ethylene oxide)
POHM	Poly(1-oxoheptamethylene)
PISE	Polymer-in-salt electrolyte
PTMC	Poly(trimethylene carbonate)
PTeMC	Poly(tetramethylene carbonate)
RDF	Radial distribution function
RF	Reference frame
SEI	Solid electrolyte interphase
SPE	Solid polymer electrolyte
SSIP	Solvent separated ion-pairs
TFSI	bis(trifluoromethane)sulfonimide
vdW	van der Waals
VFT	Vogel-Fulcher-Tammann

1. Introduction

1.1 Polymer electrolytes in Li-ion batteries

Since Sony's commercial introduction of Li-ion batteries (LIBs) in 1991, LIBs have improved vastly in performance, energy and power density, capacity, and life span[1–3]. The impact of LIBs in real life, from energy banks to cell phones, cameras, electric vehicles[4], and many more applications[5], has been recognized by the award of the Nobel Prize in 2019[6]. Although tremendous technological development has been seen in this area[7–9], LIBs still suffer from serious safety risks such as battery explosions, as seen in some Samsung phones[10] and Tesla cars[11]. One of the issues behind this is the use of liquid electrolytes in almost all commercial LIBs[12,13]. These liquid electrolytes generally consist of lithium salts dissolved in low molecular weight organic solvents such as ethylene, propylene, and diethylene carbonates that are highly inflammable[14,15,16,17]. The use of liquid electrolytes is also associated with issues such as short circuits due to the formation of Li dendrites during battery cycling[18]. One way to address these safety problems is to replace the liquid electrolytes with solid-state counterparts[19–21]; see Fig. 1.1.

Solid-state electrolytes can be classified into two main categories: ceramic and polymer electrolytes. Ceramic or inorganic solid electrolytes are mostly metal oxides, sulfides, or phosphates-based materials that are mechanically strong to prevent dendrites and can show ionic conductivities similar to liquid electrolytes[22]. But these materials are not flexible due to high brittleness, and they also face challenges regarding the poor interfacial compatibility with the battery electrodes[23]. On the other hand, solid polymer electrolytes (SPEs) possess properties that generally fall in between ceramic and liquid electrolytes

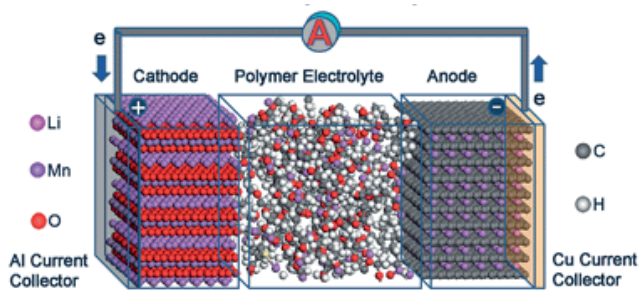

Figure 1.1: Illustration of a Li-ion battery with solid polymer electrolyte. Reproduced from Ref. [26] with permission of The Royal Society of Chemistry.

in terms of mechanical stability, flexibility, and electrode wettability but are typically limited by their low ionic conductivity at ambient temperatures[24–26].

A solid polymer electrolyte is generally defined as a solvent-free electrolyte with dissolved salt (often a Li-salt) in a polymer host material that conducts ions through the polymer matrix. Poly(ethylene oxide) (PEO) was the first solid-state polymer in which the ionic conductivity was measured through a dissolved salt by Wright and coworkers[27,28]. This was followed by Armand[29] who promoted using Li-based SPEs for Li-metal and Li-ion batteries. However, it is known that the required LIB conductivity (>10^{-3} S cm^{-1}) can only be reached for PEO-based SPEs at temperatures in the range of 80-100 °C. These electrolytes behave like 'soft solids' at these temperatures and lose much of their mechanical rigidity. The low ionic conductivity at room temperature can mainly be attributed to the presence of crystallites in the polymer network. This can be improved by adding a liquid component to SPEs, forming a gel-polymer electrolyte type (also known as a 'quasi-solid state' polymer electrolyte)[30]. However, these materials often suffer from similar problems as those of a conventional liquid electrolyte regarding safety and electrochemical stability. There are, however, many other ways to enhance the ionic conductivity in SPEs by reducing the percentage of crystallinity, either by chemically modifying the polymer network[31], or by adding ceramic nano particles[32,33], or by using alternative host polymers such as polycarbonates, polyesters, etc.[34] This calls for understanding the ion transport mechanism in SPEs and unveiling different factors that affect it.

1.2 Ion transport in polymer electrolytes

The ion transport mechanisms in SPEs are controlled by the complexity of the structure and dynamics of the polymer networks. To some degree, these motions can be understood using free volume theory[35,36]. The polymer chains are in a state of local segmental motion, resulting in an availability of free volume in the direct vicinity of the moving chain segment. This free volume provides

the opportunity for intermolecular coordination of lithium cations, eventually resulting in ions transferring from one coordination site to another by breaking and forming Li-oxygen bonds (Fig. 1.2a, b). Since the movement of ions is directly dependent on the movement of the chain segments, one can say that ion transport is coupled to polymer segmental motion[37–39]. Depending on the evolution of these coordination environments, ion transport can be distinguished by three main modes[40] i) ion hopping between distinct coordination sites (Fig. 1.2a), ii) a continuous mode, where the ion moves by successive exchanges of coordinating groups (Fig. 1.2b), and iii) ion-polymer co-diffusion – in a similar fashion to the vehicular mode, with no change of coordination environment (Fig. 1.2c). Importantly, the term "ion hopping", often used in this context, differs from the ion hopping between stationary coordination sites because of the coupling between ion dynamics and polymer dynamics. In the case of the vehicular mode, the ions are transported along with their coordination environment. However, since the polymer solvent is macroscopically immobile, vehicular mobility cannot constitute any profound macroscopic transport of cations, but only locally on the scale where the macromolecules can diffuse. Here, for the coupled (continuous) ion transport, the ionic conductivity is limited by the slow polymer dynamics. Decoupling ion transport with segmental mobility is thus a route to achieve higher ionic conductivities, which is sometimes the case also for polymers possessing rigid chain structures[41,42].

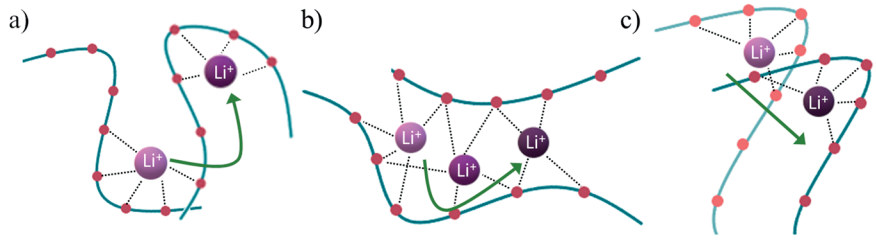

Figure 1.2: Visualization of the three ion transport modes (a) ion hopping (b) continuous mode, and (c) vehicular mode.

The differences between coupled and decoupled ion transport can be seen from the temperature (T) dependence of ionic conductivity (σ). For decoupled transport, this follows a classical Arrhenius relation, i.e., $log\ \sigma \propto 1/T$, while for the coupled transport, it follows a Vogel-Fulcher-Tammann (VFT) behavior, i.e., $log\ \sigma \propto 1/(T - T_0)$ where T_0 is the Vogel temperature[43]. T_0 is experimentally found ca. 50 K below glass transition temperature (T_g). The latter refers to a temperature where the polymer goes from a rigid and glassy state to a rubbery state, i.e., where the segmental mobility allows free rotations around the molecular axis. As discussed above regarding free volume theory: since the conduction of ions is highly coupled to the segmental motion of polymer chains, it is generally accepted that a low T_g is necessary for SPEs with

high conductivity. However, if the ion transport is decoupled from segmental relaxation,[40,41] it is possible to reach high ionic conductivity even with a high T_g.

The ion transport mechanisms in polymer electrolytes depend on various factors such as solvent polarity, molecular weight, salt concentration, functional groups, end/side-chain groups, etc. The investigation of these different factors in SPEs with molecular modeling is the focus of this thesis.

The solvent polarity of the system is a crucial factor as it determines the distribution of free Li-ions, contact, and solvent-separated ion pairs. This is one of the key factors investigated in this thesis (**Papers I** and **II**). At high solvent polarity, a strong ion-polymer interaction will result in solvated free ions being favored, whereas in a system with a low solvent polarity, ion-ion interactions will be more favorable and lead to more ion-pairs or larger aggregates. The idea that the formation of charge-neutral ion pairs (i.e., cation-anion pairs) negatively affects the ionic conductivity was introduced early on in electrolyte theory by Arrhenius. But the contribution to the total ionic conductivity from cation-anion correlations – i.e., directional correlations between the movements of distinct cations and anions (See Fig. 2.2) – is often found to be positive in different types of electrolyte systems ranging from aqueous electrolyte solutions[5] to ionic liquids[44,45,46]. This shows the necessity to understand the difference between ion-pairing and the ion-ion correlation.

Along with ionic conductivity, another key property to understanding ion transport is the transference number (t_+), which is defined as the ratio of the electric current derived from the cation to the total electric current. The transference number ideally varies from 0 to 1, and the higher the number higher the contribution of cation transport to the total ionic conductivity. Recent experimental studies have shown negative t_+ values for PEO-based SPEs[47,48], implying that cations were transported to the positive electrode. The molecular origins of this phenomenon have been explored in **Paper III**.

Another two factors that have a significant influence on ion transport mechanisms are molecular weight and salt concentration. As molecular weights gradually increase, vehicular transport is expected to gradually transition to coupled/continuous ion transport[49]. This change in transport mechanisms is also reflected in the apparent transference number t_+^{app} estimated from diffusion coefficients. It is known that t_+^{app} decrease with the increase of the molecular weight because cation transport is restricted due to slow polymer dynamics [49]. Up to a certain limit, with increasing salt concentration, the ionic conductivity increases as more charge carriers are introduced. When adding more salt, the solvation of ions in the polymer chains will form physical cross-links, which restricts the segmental motion of the polymers. As a result, the T_g increases, and the ionic conductivity reaches a maximum at a moderate salt concentration[50]. With an even further increase in the salt concentration, the cations and anions will aggregate and form clusters. This domain of the SPE phase diagram is also known as the polymer-in-salt electrolyte (PISE)[51]. These

materials often display decoupled ion transport where the transport mechanism is suggested to follow the continuous exchange of anions, like in ionic liquids[52]. The interplay between molecular weight and salt concentration is explored in **Paper IV**.

Apart from the physical conditions mentioned above, the chemistry of the ion coordinating functional groups clearly plays an important role. In **Paper V**, the transport properties of three different types of carbonyl-coordinating polymers are studied: namely polycarbonates, polyesters, and polyketones. These polymers are structurally similar, with only the functional group being different, thereby giving direct insights into the role of the non-coordinating main-chain oxygens. Both experimental techniques and molecular modeling were applied to shed the light on the changes in the coordinating environment of these carbonyl-containing polymers.

Because the above factors that control SPE behavior are highly interrelated, understanding the coupling between these factors, disentangling their contributions to ion transportation, and using this knowledge for designing new types of SPEs, constitute a grand challenge in the field. To this end, molecular modeling can provide significant aid since these aspects can be studied systematically.

1.3 Molecular modeling of SPE

SPEs involve various length and time scales, where different levels of theory and computational methodologies can be applied (see Fig. 1.3). Depending on the specified problem (i.e., the desired properties under study) and limitations

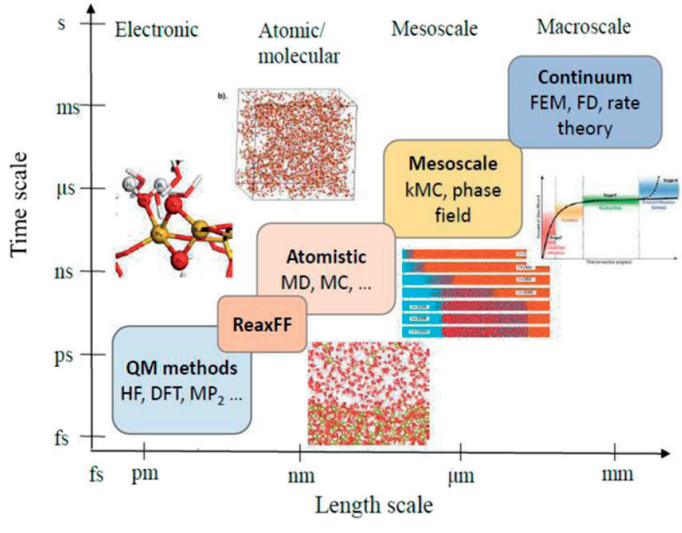

Figure 1.3: Multiscale simulation methods at various length and time scales. Reproduced from Ref. [123].

of computational resources one must choose the applied method/s accordingly. The *ab initio* quantum mechanical (QM) methods have a high level of accuracy in predicting the equilibrium structures and interaction energies but are limited to small systems (~ a few hundred atoms) as they are computationally expensive. However, density functional theory (DFT) methods are commonly employed in SPE systems to study the interactions between different salts and polymers and predict the right combinations to promote ionic mobility[53]. DFT calculations are also used to determine the electrochemical stability window of the electrolytes, i.e., whether the electrolyte is electrochemically stable at the potentials of the redox processes at the electrodes[54].

To study the ion and polymer dynamical properties in SPEs – macromolecular systems characterized by slow dynamics – larger system sizes and longer time scales are essential. So, classical molecular dynamics (MD) simulations are commonly employed to calculate diffusion coefficients, ionic conductivities and to capture structure-dynamic relationships on a time scale of a few hundred nanoseconds. However, despite the improvements in length and time scales, classical all-atom MD may still be limited when studying processes in the mesoscopic domain of micrometers and micro- to milliseconds[55]. To address this challenge, coarse-grain (CG) models can be introduced where a small group of atoms or monomer units in polymer systems can be treated as single particles. Another way is to utilize kinetic Monte Carlo (kMC) simulations that rely on sufficient sampling of the percolating path in MD simulations and extend the trajectories to a longer time scale[56].

To simulate the entire battery cell, relevant processes inside the cell (transport of lithium, reaction kinetics, and thermodynamics of both electrode and electrolytes) are commonly described analytically (using partial differential equations) and solved using, for example, Finite Element Methodology (FEM)[57]. In these models, the polymer electrolytes are approximated with a specific ionic conductivity value obtained either from previous experiments or from MD/kMC simulations. These simulations are generally used to study discharge characteristics and concentration build-up and to describe SEI growth and its ion transport[58,59].

A single computational method is not sufficient to model the complex multiscale processes in LIB. Therefore, using a multiscale approach by combining different computational methods is necessary and has been a topic of interest recently[60,61]. However, in this thesis, classical all-atom MD simulations have been utilized as they can reasonably describe the local solvation environments and ion dynamics.

1.4 Current state-of-the-art of polymer electrolyte simulations

The bulk of computational work on SPE systems has employed MD simulations, most likely since the time and length scales employed can address the most critical phenomena of ionic transport. This is also the main methodology used in this thesis work. Several of the main questions addressed here have thereby been studied before using similar techniques, and the work builds upon these previous efforts.

MD simulations have, for example, been performed to study the dependence of polymer polarity on ionic conductivity[62]. These simulations could qualitatively reproduce the experimental trends and attribute the increased ionic conductivity at high solvent polarity to an ameliorated ion aggregation and more free charge carriers. This particular study was followed by coarse-grained simulations using a Stockmayer model for PEO-based electrolytes[63,64]. Therein, the point dipole moment of the EO monomer was scaled as an indicator of the solvent polarity strength. It was found that the ionic conductivity reaches a maximum at an intermediate dipole strength. This optimal point was rationalized as a trade-off between ionic aggregation at the low polarity and slow polymer segmental dynamics at the high polarity. However, the polarity of polymer electrolytes involves both the dielectric effect and the bond polarity (effect of local coordination)[65]. Moreover, the effect that the increased polymer dielectric constant leads to enhanced ionic conductivity may be solely attributed to the shift in T_g[66]. Therefore, a fully atomistic picture beyond coarse-grained models is needed to understand the effects of polarity on ion transport, ion pairing, and ion-ion correlations (**Papers I** and **II**).

The experimentally observed negative transference numbers have been generally attributed to the formation of ion aggregates, especially negatively charged triplets (cation surrounded by two anions) and like ion-ion correlations as observed from MD simulations[67,68]. However, only marginally negative values were observed in these simulations, and the differences in the reference frames between experiments and simulations are often overlooked[69]. **Paper III** tries to fill this conceptual gap between experiments and simulations and attempts to understand this phenomenon.

The ion transport mechanisms have been well explored using MD simulations and the literature definitions of these mechanisms differ slightly[37–39]. The ion hopping and continuous motions from Fig. 1.2 are generally divided into inter-segmental and intra-segmental motions/hopping. Using these definitions, a reasonable model based on the phenomenological dynamic bond percolation (DBP)[70] and Rouse theory was proposed, which agrees with experimental results[37,39]. In subsequent studies[38,39], this model was extended by defining a time scale for each mechanism. The inter-chain hopping is then described as a renewal process similar to the DBP model, and the other two as

motions coupled to the polymer segmental dynamics, which are therefore describable within the framework of the Rouse model. These studies point out that segmental polymer dynamics play a critical role in influencing the transport of both anions and cations and that inter-chain hopping is crucial for fast cation transport. However, it has also been shown that inter-chain jumps occur with a low frequency and intra-chain transport is the dominant transport mechanism in PEO-based SPEs [49,71,72]. Thus, even if inter-chain hopping is the faster transport mechanism, it is restricted due to the high activation barrier for this movement. The relative proportions of the different transport modes in terms of hopping and alternative mechanisms are often not quantified, even in theoretical works. **Paper IV** attempts to quantify these mechanisms where all the interactions between cation, anion, and polymer are considered.

The bulk part of this thesis focuses on ether-based polymers, i.e., PEO-based SPEs. However, PEO is known to have a high coordination strength to lithium, leading to low transference numbers, especially at high molecular weights. Therefore, a host material with a weaker coordination strength is desired for a high transference number. For example, carbonyl-containing polymers such as polyketones, polyesters, or polycarbonates exhibit lower coordination strengths compared to the ether group[34,73]. A recent DFT study showed a higher coordination strength for systems with more ester groups in a series of polyester-polycarbonate copolymer systems[74]. However, these calculations were performed on oligomeric systems due to their limited length and time scales in DFT calculations. So, the MD simulations in **Paper V** could provide a more realistic relationship between the local coordination environment and coordination strength in polymeric systems.

1.5 Scope of this thesis

This thesis's main goal comprises understanding the complex ion transport mechanisms in solid polymer electrolytes (SPEs) using all-atom Molecular Dynamics (MD) simulations. While ion transport in SPEs has been explored for decades, there are still gaps between experimental and computational studies. The results from the five papers in this thesis try to fill these gaps by critically examining the relationships between different properties in SPE systems: polarity, coordination, ion-pairing, and ion-ion correlations, which highly influence the ionic transport mechanism.

Papers I and **II** investigated the relationship between polarity, ion-pairing, and ion-ion correlations. The solvent polarity (ε_p) of poly(ethylene oxide) (PEO) doped with the LiTFSI system is modulated using a charge scaling method. A method to separate the effects of solvent polarity and glass transition temperature is proposed. A maximum in the Li-ion diffusion coefficient with respect to ε_p is observed. To understand this trend, polymer dynamics, ion-transport mechanisms, and local solvation environments were studied. It

is then shown that the optimal solvating ability of Li-ion at intermediate values of ε_p lead to fast ion conduction. Additionally, the solvent polarity modulates the formation of charge-neutral ion pairs, which is commonly considered detrimental for ionic conductivity. The relation between cation−anion distinct conductivity and the lifetime of ion pairs was examined to study their contribution to the total ionic conductivity.

Paper III scrutinized the origins of the recently observed negative transference numbers. The effect of choice of reference frames (barycentric and solvent-fixed) on the transference number and Onsager coefficients were investigated. The difference in ion-ion correlations observed for reference frames could explain the differences between experiments and computations.

Paper IV investigated the relationship between coordination chemistry, ion transport mechanisms, and conduction properties by comparing PEO and polyester-based SPEs. A quantitative method was proposed based on the cation coordination change with polymers and anions. The correlation between transport mechanisms and cation transport was then studied at different molecular weights and salt concentrations. Finally, **Paper V** investigated the coordination and ionic transport properties of three resemblant carbonyl-coordinating polymers: polyketones, polyesters, and polycarbonates. The role of extra main-chain oxygens for the latter polymers was then investigated by studying the electrostatic energy between the Li-ion and the carbonyl group and the cationic transference numbers.

2. Theoretical background

2.1 Molecular dynamics simulations

Richard Feynman said in 1963 that "everything that living things do can be understood in terms of the jiggling and wiggling of atoms." [75] MD are computer simulations to observe the motion of interacting particles as a function of time by solving Newton's equations of motions – i.e., their very "jiggling and wiggling". The forces between the interacting particles can be fairly accurately determined using first principles calculations known as ab-initio MD (AIMD), where the electronic structure of the system is solved at every time step.[76] AIMD simulations with density functional theory (DFT) is a common approach to study the structure and dynamics of water or other hydrogen-bonded liquids on different solid surfaces[77–79], mechanisms of surface catalytic processes with industrial and biological applications[80,81], and also polymer degradation mechanisms in Li-ion batteries[82]. However, these simulations are limited to systems comprising several hundred atoms and time scales of the order of a few 100 ps as they are highly computationally expensive. To reach larger system sizes and longer time scales, empirical force fields can be used where the atoms are approximated as spherical balls with a point charge; these simulations are known as classical MD. This approximation allows simulating systems with hundreds of thousands of particles with time scales varying from a few nanoseconds to microseconds. MD simulations have been used to study a wide range of properties, including biological systems such as protein folding or ligand bindings at the atomistic level[83,84]. It is also a widely used computational method to study the properties of nanoparticles, self-assembled systems, phase transitions, and structural and thermal properties of glasses. It can also provide insights into the dynamics of polymer electrolyte systems. In this section, basic principles and standard algorithms used in MD simulations are summarized[85].

In MD simulations, the trajectories are generated by numerically integrating Newton's equations of motion[86]:

$$m_i \frac{\partial^2 \boldsymbol{r_i}}{\partial t^2} = \boldsymbol{F_i} = -\partial V / \partial \boldsymbol{r_i} \tag{2.1}$$

where $\boldsymbol{F_i}$ is the force acting on atom *i*, V is the total interaction energy of the system, $\boldsymbol{r_i}$ is the position vector of atom *i*, and m_i is the mass of atom *i*. These forces generally depend on the particles' positions, which will change

whenever particles move or interact. This requires a continuous sequence of states updated with time, i.e. from the current state of atom ($\boldsymbol{r}(t)$, $\boldsymbol{v}(t)$) to the next state ($\boldsymbol{r}(t + \delta t)$, $\boldsymbol{v}(t + \delta t)$). These positions and velocities are integrated using the finite difference method, which assumes that these can be approximated as Taylor series expressions. The basic functionality of the finite difference method is that the integration is broken down into many small stages, each separated in time by a fixed time step δt. In the first stage, the total force on each particle in the configuration at a time t is determined, and then in the second stage, the accelerations of the particles can be calculated from the force. Finally, the obtained accelerations are combined with the positions and velocities at time t to calculate the positions and velocities at time $t + \delta t$. One of the simplest algorithms to solve Newton's equations of motion is the Verlet algorithm. This algorithm uses the positions and accelerations at time t, and the positions at ($t - \delta t$), to calculate new positions at a time ($t + \delta t$).

$$\boldsymbol{r}(t + \delta t) = \boldsymbol{r}(t) + \boldsymbol{v}(t)\delta t + \frac{1}{2}\boldsymbol{a}(t)\delta t^2 + \cdots \tag{2.2}$$

$$\boldsymbol{r}(t - \delta t) = \boldsymbol{r}(t) - \boldsymbol{v}(t)\delta t + \frac{1}{2}\boldsymbol{a}(t)\delta t^2 + \cdots \tag{2.3}$$

By adding Eq. 2.2 and Eq. 2.3, the positions at a time ($t+ \delta t$) can be calculated as,

$$\boldsymbol{r}(t + \delta t) = 2\boldsymbol{r}(t) - \boldsymbol{r}(t - \delta t) + \boldsymbol{a}(t)\delta t^2 \tag{2.4}$$

To obtain velocities, the difference between Eq. 2.2 and Eq. 2.3 is used:

$$\boldsymbol{v}(t + \delta t) = \frac{\boldsymbol{r}(t + \delta t) - \boldsymbol{r}(t - \delta t)}{2\delta t} \tag{2.5}$$

So, the coordinates of the new positions $(t + \delta t)$ and the old positions $(t - \delta t)$ are needed to calculate the velocities at $+\delta t$. Therefore, the initial velocities need to be estimated, which indicates that the method is not entirely self-reliant. To overcome this limitation, there are several variations and algorithms which have improved upon the Verlet scheme. One of the modified Verlet schemes in which the velocities appear explicitly is the so-called leap-frog algorithm:

$$\boldsymbol{r}(t + \delta t) = \boldsymbol{r}(t) + \boldsymbol{v}\left(t + \frac{1}{2}\delta t\right)\delta t \tag{2.6}$$

$$\boldsymbol{v}\left(t + \frac{1}{2}\delta t\right) = \boldsymbol{v}\left(t - \frac{1}{2}\delta t\right) + \boldsymbol{a}(t)\delta t \tag{2.7}$$

The size of the time step determines the stability of any algorithm used. Therefore, it must be an order of magnitude smaller than the fastest motions taking place in the system. Typically for SPEs, this would be the vibration of a bond that involves a hydrogen atom, and consequently, the time step should

be a maximum of the order of 1 fs. Small time steps will thus lead to insufficient phase space sampling, whereas large time steps will lead to instabilities in the integration algorithm and high energy overlaps. So, a trade-off between accuracy and computational economy exists.

An ensemble characterizes a particular thermodynamic state. An ensemble is a collection of systems belonging to a single macroscopic state with different microscopic states. In MD simulations, widely used ensembles are NVT (fixed number of atoms, N, fixed volume, V, and fixed temperature, T), NPT (N, P, and Temperature is fixed), NVE (N, V, and energy are fixed).In NVT and NPT ensembles, a thermostat procedure can be applied in which the system is coupled to a heat bath, and the energy of the system consequently changes gradually with a suitable time constant. A coupling parameter τ controls the rate of the heat transfer:

$$\frac{dT}{dt} = \frac{1}{\tau}\,(T_0 - T) \tag{2.8}$$

where T_0 is the desired temperature, and T is the instantaneous temperature. Some of the most common temperature scaling methods are the Berendsen thermostat[87], velocity-rescaling thermostat (Bussi-Donadio-Parrinello thermostat)[88], Andersen thermostat[89], and Nosé-Hoover thermostat[90,91]. In Berendsen's thermostat, velocities are rescaled to adjust the kinetic energy of the system, and the velocity scale factor is given as:

$$\lambda = \left(1 + \frac{\delta t}{\tau}\left(\frac{T_0}{T} - 1\right)\right)^{\frac{1}{2}} \tag{2.9}$$

The velocity-rescaling thermostat is essentially a Berendsen thermostat with an additional stochastic term that ensures a correct kinetic energy distribution. Moreover, a barostat method can be applied to maintain the system's pressure constant by coupling it to a pressure bath. In this case, the volume of the system is changed by scaling all coordinates:

$$\frac{dP}{dt} = \frac{1}{\tau}\,(P_0 - P) \tag{2.10}$$

where P_0 is the desired pressure, and P is instantaneous pressure. The scaling factor for the box vectors to scale the volume is given as:

$$\mu = \left(1 + \frac{\delta t}{\tau}\,\kappa(P_0 - P)\right)^{\frac{1}{3}} \tag{2.11}$$

where κ is the compressibility constant of the system. Two common methods for pressure coupling are those of Berendsen and Parrinello-Rahman[92].

2.2 Force fields

In MD simulations, a force field defines the potential energy function V which governs the interactions between atoms. This V consists of terms characterizing different interactions of the system. The functional form of the force fields is a trade-off between accuracy in representing forces acting on atoms and the computational cost. Potential terms for both bonded and non-bonded interactions are defined and contained in these force fields, where the former includes bond, angle, dihedral, and improper interaction terms, while the latter includes van der Waals (vdW) and electrostatic interaction terms. A typical MD potential is of the following form:

$$V = \sum_{bonds} \frac{1}{2} k_b (r - r_0)^2 + \sum_{angles} \frac{1}{2} k_b (\theta - \theta_0)^2 + \sum_{dihedrals} k_\phi (1 + \cos(n\phi - \phi_s)) + \sum_{improper} \frac{1}{2} k_\xi (\xi - \xi_0)^2 + \sum_{vdw} 4\epsilon_{ij} \left(\frac{\sigma_{ij}^{12}}{r_{ij}^{12}} - \frac{\sigma_{ij}^{6}}{r_{ij}^{6}} \right) + \sum_{ele} \frac{1}{4\pi\varepsilon_0 \varepsilon} \frac{q_i q_j}{r_{ij}} \quad (2.12)$$

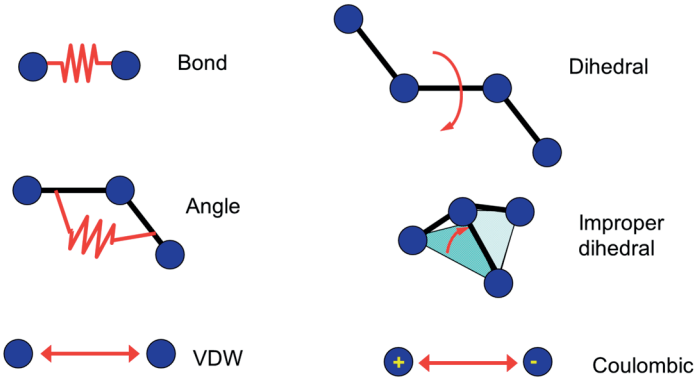

Figure 2.1: Illustration of bonded and non-bonded interactions in a typical MD potential. Reproduced from Ref. [124].

In general, force fields can be classified into three classes depending on the number of potential terms and their functional forms. In class I force fields, intramolecular interactions are represented by harmonic potentials and intermolecular interactions by Lennard-Jones 6-12 and Coulomb terms based on atomic charges. Several force field papramerter libraries are established in this category: AMBER, General AMBER, GROMOS, OPLS, CHARMM, etc. All of these derive force constants and geometrical parameters from QM calculations and experimental measurements like vibrational bond-spectra or melting points of solvents and mainly differ in the derivation of the parameters.

In class II force fields, the bonded interactions can be represented in anharmonic terms such as Morse potentials or higher-order terms beyond the harmonic to improve the description of bond stretching/compression energies. Equilibrium bond lengths are coupled to bond angles and torsional energies in real systems. Such coupling terms can be introduced in these force fields to consider the interdependence of bonds and angles, bonds and torsions, or angle and torsions. Alternative forms for non-bonded interactions such as Buckingham potential for the vdW interactions are also used in some force fields. The MMFF94, MM3 and UFF force fields generally fall into this category.

The partial charges in the electrostatic term can be derived either from a fit to experimental thermodynamic data (for small molecules) or by performing ab initio calculations. Furthermore, the charge distribution within a molecule – and therefore its electrostatic potential – depends on the molecular conformation and the chemical environment. Thus, not only is there no unique solution to the problem of determining partial atomic charges, but the electrostatic interactions should also depend on the molecule's conformation and its environment[93]. This problem can be tackled by the so-called 'polarizable force fields' or 'next-generation force fields'. Polarization refers to the redistribution of a molecule's electron density due to an electric field exerted by other molecules. This is a non-pairwise additive interaction, so the use of effective charges to describe the average polarization is only a partial solution to this problem, reducing the transferability of the force field to other chemical systems. There are three principal methods to do this: 1. Fluctuating charge model; 2. Shell models (Drude particles); 3. Induced point dipoles. During the 1990s, the first general polarizable force fields appeared. The PIPF (polarizable intermolecular potential function), DRF90, and AMOEBA force fields are today commonly used. In addition, some of the general force fields mentioned above have also developed polarizable versions. These methods are, however, limited by high computational cost for long time-scale simulations[94]. Instead, scaling the point charges has been shown to be a practical approach to introducing electronic polarization. In simulations of polymer electrolytes, a scaling factor between 0.5 to 0.8 has been commonly used for salt ions in recent years[95–98]. For the MD simulations in **Paper I-V**, general AMBER force field parameters (GAFF)[99,100] were using to were used to describe the interactions between the polymer chains and ions. The particle charge of the ions was scaled by a factor of 0.75 to get better in accordance with the experiment.[101,102] In **Paper I** and **II**, charge scaling methods[103] have been employed not only to the salt ions but also to the polymer matrix, and their effects on polymer and ion dynamics in polymer electrolyte systems were studied subsequently.

2.3 Investigated properties

2.3.1 Bulk polymer properties

Glass transition temperature (T_g):

The glass transition temperature is where a polymer material changes from a rigid glassy material to a soft (not melted, but rubbery) material and is usually measured in terms of stiffness or modulus. The T_g of a polymer system can be determined from the change in the density values as a function of temperature:

$$\rho_g(T) = \rho_r(T)|_{T=T_g} \tag{2.13}$$

The temperature dependence of the density for a polymer in the glassy state $\rho_g(T)$ differs from that of a polymer in the rubbery state $\rho_r(T)$, which is used in MD simulations to determine T_g. The tangents of these two functions intersect at one temperature, which gives the T_g. Importantly, the calculation of T_g is highly dependent on the choice of force fields used in the MD simulations.

Dielectric constant:

The dielectric constant can be defined as a measure of a solvent's ability to screen charges from each other and reflects the strength of solvent polarity. In non-polarizable MD simulations, the static dielectric constant ε_s of the system can be calculated from the relations (where $\varepsilon_\infty = 1$)[104,105]

$$\varepsilon_s = 1 + \frac{4\pi}{3Vk_BT}[\langle \mathbf{M}^2 \rangle - \langle \mathbf{M} \rangle^2]. \tag{2.14}$$

Where, the dipole moment of the simulation both at time *t*, is defined as

$$\mathbf{M}(\boldsymbol{r}(\mathbf{t})) = \sum_{i=1}^{N} q_i \boldsymbol{r}_i(t)\,, \tag{2.15}$$

where N is the number of atoms in the system, $\boldsymbol{r}_i$ and q_i are the atomic position and the charge of atom *i*, respectively.

2.3.2 Structural properties of polymer electrolytes

Radial distribution functions (RDF) and Coordination numbers (CN):

The most obvious structural quantity to compute using MD is the radial distribution function, which describes on average how the atoms are radially packed around each other. It can be defined as the ratio between the local density on a spherical shell of thickness δr at a distance r from the chosen atom and the average density. The radial distribution function g(r) can be obtained by the following equations:

$$g(r) = \frac{1}{\rho N} \sum_i \sum_{j \neq i} \frac{\langle \delta(r_{ij} - r) \rangle}{4\pi r^2} \tag{2.16}$$

with ρ being the number density. The volume integral of the g(r) from zero to the first minimum after the nearest neighbor peak gives the number of direct

neighbors of each atom, i.e., the average coordination number of atoms throughout the simulation:

$$CN = 4\pi\rho \int_0^{r_{min}} r^2 g(r) dr. \tag{2.17}$$

2.3.3 Transport properties in polymer electrolytes

In dilute solutions[106], the flux of the ions ($\mathbf{J}_\alpha$) seems to arise from a single electrochemical driving force which is defined as the negative gradient of the electrochemical potential ($\mathbf{X}_\alpha = -\nabla\mu_\alpha$), thus the flux is:

$$\mathbf{J}_\alpha = -u_\alpha c_\alpha \nabla\mu_\alpha + c_\alpha \mathbf{v} \tag{2.18}$$

where, u_α is the mobility of ions, $c_\alpha$is the molar concentration of the species α and $\mathbf{v}$ is the bulk velocity (in case of convection). However, in the concentrated solutions, the interactions between different ionic species couple to the flux of these species. Those couplings can be represented by the Onsager phenomenological equation (Eq. 2.19)[107], which relates the flux $\mathbf{J}_\alpha$ of the species α to the electrochemical driving force $\mathbf{X}_\beta$ exerted on species β, through the Onsager transport coefficients $\Omega_{\alpha\beta}$.

$$\mathbf{J}_\alpha = \sum_\beta \Omega_{\alpha\beta} \mathbf{X}_\beta \tag{2.19}$$

These Onsager transport coefficients can be represented as the correlation functions of the flux densities of ions (Eq. 2.20) or its equivalent Einstein-type relation (Eq. 2.21).[108–110]

$$\Omega_{\alpha\beta} = \frac{1}{3k_B T} \int dr \int_0^\infty dt \langle \mathbf{J}_\alpha(0,0) \mathbf{J}_\beta(\mathbf{r}, t) \rangle \tag{2.20}$$

$$\Omega_{\alpha\beta} = \frac{1}{6k_B T V N_A^2 t} \langle \Delta\mathbf{r}_{\boldsymbol{\alpha}}(t) . \Delta\boldsymbol{r}_{\boldsymbol{\beta}}(t) \rangle \tag{2.21}$$

Here, N_A is the Avogadro number, $\Delta\mathbf{r}_{\boldsymbol{\alpha}}(t)$ is the total displacement of species α over a time interval t and $\langle \Delta\mathbf{r}_{\boldsymbol{\alpha}}(t) . \Delta\boldsymbol{r}_{\boldsymbol{\beta}}(t) \rangle$ is the mean-squared cross displacements (MSCD) between species α and β. The Green-Kubo (G-K) ionic conductivity (σ_{G-K}) can be expressed in terms of $\Omega_{\alpha\beta}$ (Eq. 2.22), which accounts for the different contributions arising from the correlations between ionic species.

$$\sigma_{G-K} = \sum_{\alpha\beta} q_\alpha \, q_\beta N_A^2 \Omega_{\alpha\beta} \tag{2.22}$$

Here q_α is the formal charge of species α. For a binary electrolyte system, i.e., cation (+) to anion (-) ratio is 1:1, the Eq. 2.22 can be written as

$$\sigma_{G-K} = N_A^2 \, (\, \Omega_{++} + \Omega_{--} - 2\Omega_{+-}). \tag{2.23}$$

Note that $\Omega_{\alpha\alpha}$ coefficients have two contributions: self ($\Omega_{\alpha\alpha}^s$) and distinct parts ($\Omega_{\alpha\alpha}^d$). The self-part arises from uncorrelated particle motion and is directly related to the self-diffusion coefficient of the species. The distinct part

arises when cross-correlations between two distinct particles of same or different species is considered.

$$\Omega^{s}_{\alpha\alpha} = \frac{1}{6k_B TVN_A^2 t}\langle \|\Delta \mathbf{r}_{\boldsymbol{\alpha}}(t)\|^2 \rangle = \frac{ND_\alpha}{k_B TN_A^2 V} \tag{2.24}$$

Here D_α is the self-diffusion coefficients and $\langle \|\Delta \mathbf{r}_{\boldsymbol{\alpha}}(t)\|^2 \rangle$ is the mean-square displacements (MSD) of species α. The self-terms are considered as ideal situation when ion-ion correlations are absent and could estimate the Nernst–Einstein (N-E) contributions to transport. The Eq. 2.22 with self and distinct contributions of ionic conductivity can be given as,

$$\sigma_{G-K} = \sigma_{N-E} + \sigma^{d}_{++} + \sigma^{d}_{--} + \sigma^{d}_{+-}. \tag{2.25}$$

Knowing these Onsager coefficients, one can express the cation transference number (t_+), as

$$t_+ = \frac{\Omega_{++} - \Omega_{+-}}{\Omega_{++} + \Omega_{--} - 2\Omega_{+-}} \tag{2.26}$$

and the apparent transference numbers (t_+^{app}) can also be estimated from the self-diffusion coefficients,

$$t_+^{app} = \frac{\Omega^{s}_{++}}{\Omega^{s}_{++} + \Omega^{s}_{--}} = \frac{D_+}{D_+ + D_-}. \tag{2.27}$$

3. Summary of key results and discussion

This chapter summarises the key results and discussion from **Papers I-V**. These papers focus on critically examining the relationship between different polymer electrolyte properties. All-atom MD simulations are performed using the GROMACS software package[111], and general AMBER force field (GAFF)[99,100] parameters describe the bonding and non-bonding interactions. In **Papers I-III**, the common PEO-LiTFSI (poly(ethylene oxide)-lithium bis(trifluoromethane)sulfonimide) SPE system is studied, as a prototype material. This has been well studied in numerous papers, comprising both experimental and computational work. In **Papers IV-V**, this portfolio of SPE materials is expanded, and also systems consisting of LiTFSI salt with polyketone, polyester, and polycarbonate as polymer hosts are investigated. These more novel SPE host materials have been receiving plenty of attention in recent years and are considered to challenge the PEO paradigm and open new paths for the development of SPEs[34]. These five individual papers provide somewhat different perspectives of the MD methodology itself, and on the materials at hand. **Paper I** and **II** investigate the effect on solvent polarity and ion-ion correlations and shows how MD is useful to *tune* these properties and *separate* between different factors that control ion transport. **Paper III**, in turn, focus on how the MD technique needs to be *adapted* for comparisons with relevant experimental studies. **Paper IV** *apply* MD simulations to quantify distinct ion transfer mechanisms in SPEs, and in **Paper V** MD simulation is used to *support* experimental investigations of how different polymer properties control the ionic transport parameters.

Thereby, in this summary, each section in the following discusses the relationships between different properties of these materials:

3.1 Relationship between polarity, coordination, and ionic transport

The polarity of a solvent reflects its ability to solvate the salt into cations and anions and thus directly affect the conductivity of ions. Experimentally, the solvent polarity of SPEs can be tuned by changing the polymer chemistry through side chains or backbone. However, the ionic transport could simultaneously then be affected by a corresponding change in the polymer architecture, glass transition temperature, or donor number. In **Paper I**, all-atom MD simulations are used to disentangling these factors and study the dependence of solvent polarity on coordination and cation transport. The direct relation between the solvent polarity and atomic charges is seen in Eq. 2.17 and 2.18, which suggests that solvent polarity could be modulated by scaling these charges. By varying the partial charges on both the polymer (P) and the salt (S) molecules, different systems were generated (see Table 1 in **Paper I**) to check this relation. For example, in the system $P_{1.50}S_{0.75}$, the charges on polymer and salt are scaled by factors of 1.50 and 0.75, respectively.

3.1.1 Modulation of solvent polarity

In Fig. 3.1a, the neat polymer system's solvent polarity increases with the polymer charge scaling factor from 0.45 to 1.50 ($P_{0.45}$ to $P_{1.50}$). This increase is also observed for the polymer electrolyte systems (polymer + salt), and the scaling of point charges of the salt ions ($S_{0.75}$ case) has a limited effect on the values of ε_p. This confirms that the solvent polarity can be modulated by scaling the atomic charges on the polymer.

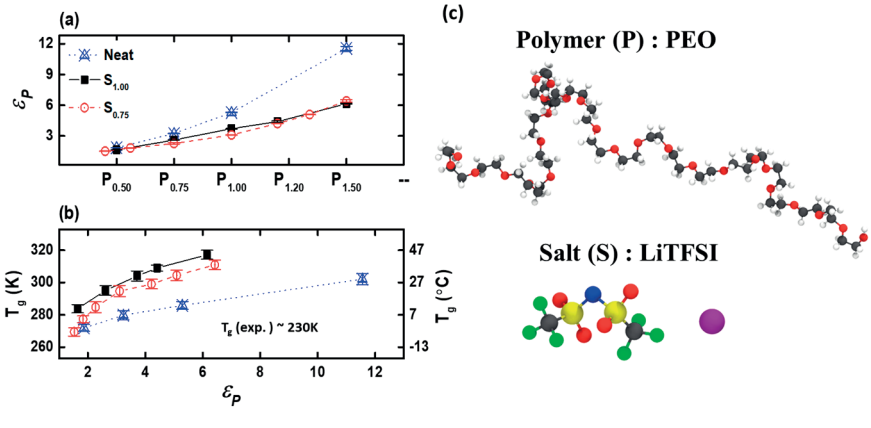

Figure 3.1: (a) The dielectric constants of PEO (ε_p) in the neat and salt-doped systems for different charge scaling schemes. (b) Tg of neat and salt-doped polymers as a function of the solvent polarity ε_p. (c) Polymer (P) and salt (S) molecules were used in the MD simulation. Adapted with permission from [102] Copyright 2022 American Chemical Society.

In Fig. 3.1b, the T_g increases with the solvent polarity ε_p due to the increased polymer-polymer interactions that reduce the free volume. The difference in T_g between the neat and LiTFSI doped systems originates from the restrictions of the polymer segmental motion with the inclusion of salt, which forms physical cross-links of the polymer chains. The weaker electrostatic interactions between the salt and the polymer chains in the $S_{0.75}$ cases lead to a lower T_g than in the $S_{1.00}$ cases. There is also a noticeable difference in the T_g between experimental and simulated systems[49]. To compensate for this, the normalized temperatures ($T - T_0$) were used to compare other properties. Here, T_0 is taken as 50 K below the T_g, which was suggested to give the best fit to experimental data[112,113].

3.1.2 Li-ion conduction and polymer dynamics

The linear relation of the self-diffusion coefficient of Li^+ (D_{Li+}) and the normalized temperature ($1000/(T-T_g+50)$) in Fig. 3.2a shows that the systems displayed VFT-type behavior and were in good agreement with experimental data[114]. When increasing the solvent polarity from $P_{0.50}$ $S_{1.00}$ to $P_{1.50}$ $S_{1.00}$, the intercept of D_{Li+} vs. ($1000/(T-T_g+50)$ becomes smaller, as well as the slope of the corresponding curve. This means that the Li^+ diffusion in these polymer electrolyte systems follows the so-called Meyer-Neldel rule in the low-to-intermediate range of ε_p, where the prefactor decreases together with the activation energy[115]. An exception was found for the highest solvent polarity ($P_{1.50}S_{1.00}$), which suggests a different ion transport mechanism, as will be discussed later.

To separate the different effects of solvent polarity and T_g, cross-sectional data for D_{Li+} at a chosen normalized inverse temperature of $1000/(T-T_g+50) \sim 5.4$ (the vertical line in Fig. 3.2a), were selected for a range of different polarities. In Fig. 3.2b, D_{Li+} at normalized temperature for both $S_{1.00}$ and $S_{0.75}$ cases increases with ε_p, reaches a maximum ε_p = 3-4, and then decreases at higher ε_p. The $S_{0.75}$ case has higher diffusion coefficients than the $S_{1.00}$ case, and this could be attributed to the introduction of electronic screening in polymer−ion and ion−ion interactions when the salt ionic charges are scaled.

In PEO-LiTFSI systems, it is known from experiments[37,116] that the magnitude of self-diffusion coefficients of each component should follow the order $D_{TFSI} >> D_{Li^+} > D_{PEO}$ during extended time scales. In Fig.3.2c, d, at high ε_p this sequence can be observed, and when the value of ε_p is low, $D_{PEO} >> D_{TFSI} \sim D_{Li^+}$ was found. This difference suggests that there is significant ion-pairing due to the poor screening from the solvent and that the diffusion of Li^+ is decoupled from the polymer matrix. In the high ε_p regime, D_{Li^+}/D_{PEO} is larger than 1, which indicates a change of transport mechanisms

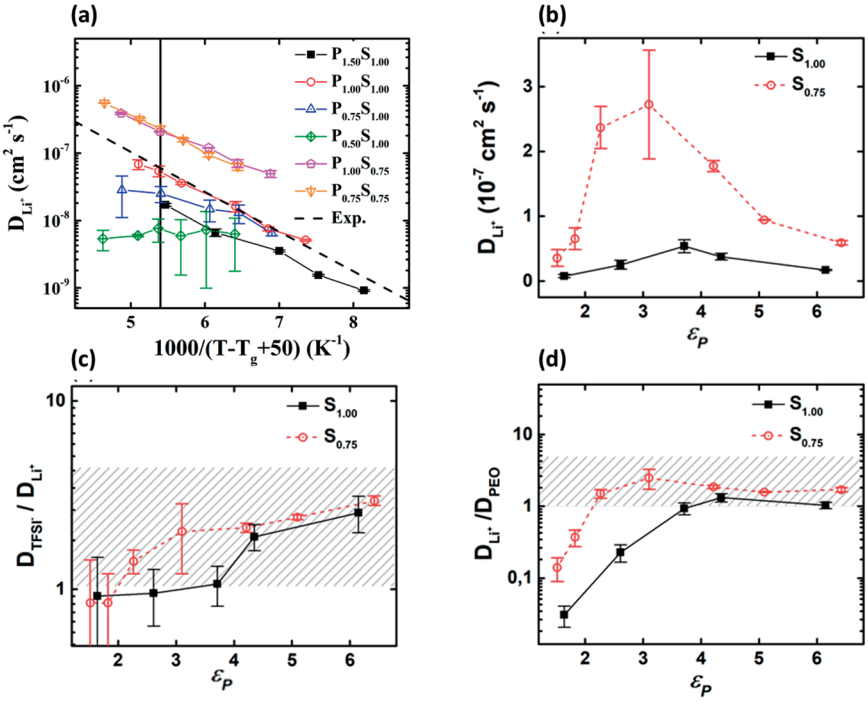

Figure 3.2: (a) Li^+ self-diffusion coefficient (D_{Li^+}) as a function of normalized inverse temperature for different charge scaling schemes. The experimental line was taken from Ref. [114]. (b) Li^+ self-diffusion coefficient (D_{Li^+}), (c) D_{TFSI}/D_{Li^+}, and (d) D_{Li^+}/D_{PEO} as a function of solvent polarity at the normalized inverse temperature $1000/(T\text{-}T_g+50)$ of 5.4 (± 0.1). Grey region corresponds to the expected values $D_{TFSI}/D_{Li^+} > 1$, and $D_{Li^+}/D_{PEO} > 1$. Adapted with permission from [102] Copyright 2022 American Chemical Society.

3.1.3 Li-ion transport mechanisms

These observations indicate that the Li-ion transport mechanisms vary with the solvent polarity ε_p. The local solvation environment was tracked for the entire trajectory to investigate these mechanisms. The indices of PEO chains (1-200) within the first solvation shell for Li-O(PEO) were recorded every time step. The time evolution of these indices for a random Li^+, for systems with high, intermediate, and low solvent polarity are presented in Fig. 3.3a, c, d for the $S_{1.00}$ case and in Fig. 3.3b, d, f for the $S_{0.75}$ case.

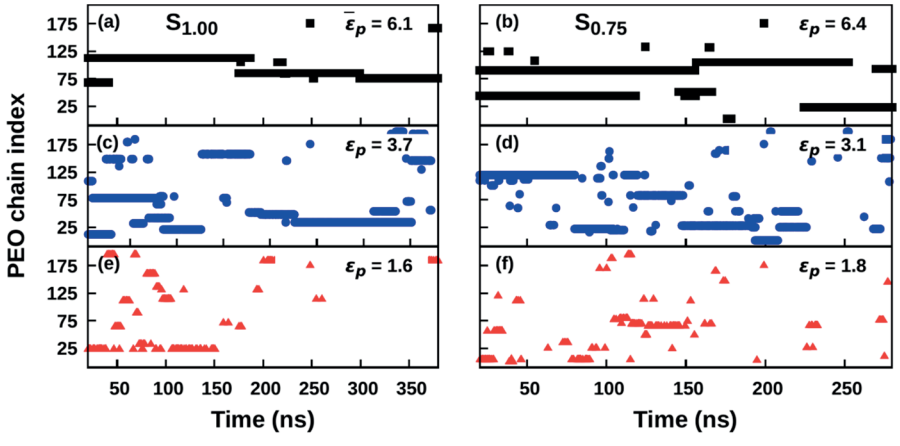

Figure 3.3: Li^+-PEO chain coordination environments as a function of simulation time for the $S_{1.00}$ cases at ε_p = 6.1(a), 3.7(c), 1.6(e) and for the $S_{0.75}$ cases at ε_p = 6.4(b), 3.1(d), 1.8(f). One visit is counted if Li^+ stays with that PEO chain for more than 5% of simulation time (~ 20-30 ns). Adapted with permission from [102] Copyright 2022 American Chemical Society.

From Fig. 3.3a, b at high ε_p, Li^+ ions typically stay with one or two PEO chains for more than 100 ns and then move to another chain. In this case, the dominated transport was mainly intra-chain diffusion, either as hopping between different oxygens on the same chain or through segmental motion. At intermediate ε_p (maximum D_{Li^+}), the inter-segmental motions between different PEO molecules becomes much more frequent (Fig. 3.3c, d). Finally, at low ε_p, the Li^+ ions seem to be barely coordinated to the PEO chains, suggesting that they are primarily coordinated to TFSI ions (Fig. 3.3e, f). This shows a transition of the transport mechanism from a vehicular mechanism at low ε_p to the frequent inter-segmental motions at intermediate ε_p and to the intra-segmental motions at high ε_p for both the $S_{1.00}$ and $S_{0.75}$ cases.

3.1.4 Local coordination vs. Li-ion transport

The calculated CNs for Li^+-O(PEO) and Li^+-O(TFSI) in different polarization environments are plotted in Fig. 3.4b, along with the respective diffusion coefficients. At lower solvent polarity, Li^+ is mostly coordinated by TFSI for both $S_{1.00}$ and $S_{0.75}$ cases (also see the snapshot in Fig. 3.4a). As the solvent polarity increases, there is a cross-over in CNs of Li^+-O(PEO) and Li^+-O(TFSI) for both $S_{1.00}$ and $S_{0.75}$ (which were also illustrated in Fig. 3.4a, d, c, and e). The CN of Li^+-O(TFSI) is negligible at high solvent polarity, which indicates that Li^+ is mostly coordinated by the polymer matrix (the snapshot in Fig. 3.4e). Interestingly, the maximum D_{Li^+} shows up when the coordination of Li-ion involves both PEO and TFSI (the snapshots in Fig. 3.4c, d). This suggests that an optimal solvating ability of polymer functional groups is crucial for fast Li-ion conduction in SPEs.

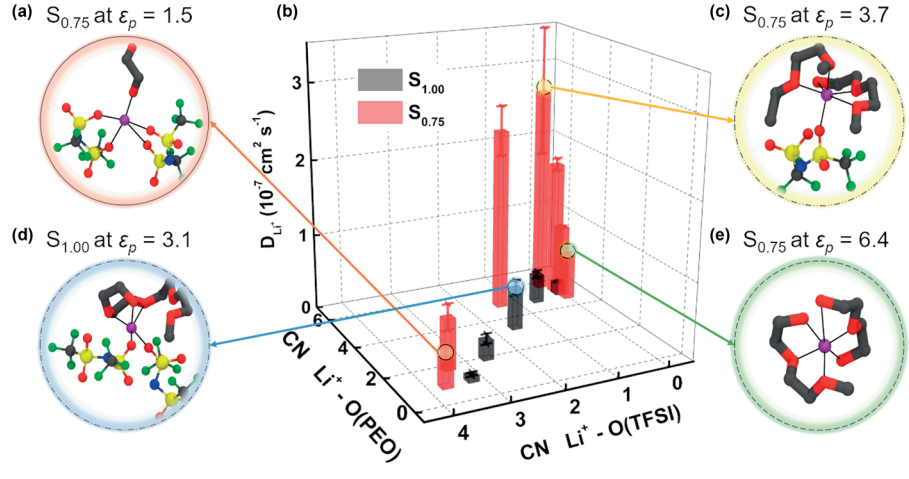

Figure 3.4: 3D bar plot of D_{Li^+} as function of coordination numbers (CNs) of Li^+-O(PEO) (bottom left axis) and Li^+-O(TFSI) (bottom right axis) at the normalized inverse temperature $1000/(T\text{-}T_g{+}50)$ of 5.4 (± 0.1). Representative snapshots of the first coordination shell of Li^+ in different polarization environments are also shown. These snapshots show the cross-over in Li^+ coordination environment from TFSI to PEO with an increase in the solvent polarity. Color coding of atoms: Li-violet, C-grey, N-blue, O-red, F-green, and S-yellow. Reproduced with permission from [102] Copyright 2022 American Chemical Society.

The balanced interactions between the Li-ions with TSFI and PEO facilitate the interchain transfer among the PEO chains, as seen from Fig. 6 in **Paper I**. However, the Li^+ is mostly coordinated to the same TFSI ions in the case of $S_{1.00}$, whereas it moves between different TFSI ions in the case of $S_{0.75}$. This difference leads to higher diffusion coefficients for $S_{0.75}$ and could be attributed to the effect of electronic polarization through charge scaling of the salt.

3.2 Relationship between polarity and ion pairing

In **Paper I**, D_{TFSI}~D_{Li^+} at low solvent polarity, and the high CN of Li^+-O(TFSI) hints at the presence of ion pairing in this regime. Bjerrum's criterion also suggests that solvent polarity plays a critical role in forming ion pairs, distinguishing between contact ion pairs (CIPs) and solvent-separated ion pairs (SSIPs). The general conception is that the presence of charge-neutral ion pairs decreases the total ionic conductivity. However, Bjerrum's convention is a thermodynamic criterion, while ionic conductivity is a dynamical property; therefore, the lifetime of these ion pairs should be considered when discussing the contribution of ion pairing to ionic conductivity. In **Paper II**, the dependence of solvent polarity on ion paring and the importance of its lifetime were studied. Here only the $S_{0.75}$ case is used as it has enhanced ion dynamics, while both $S_{1.00}$ and $S_{0.75}$ cases show a similar trend as a function of solvent polarity.

3.2.1 The modulation of ion pairing

The g(r) of Li−N(TFSI) are plotted in Fig. 3.5a, where it can be observed that the first and second peaks decrease with an increase in the solvent polarity. Furthermore, the fraction of Li-ions that form CIPs in the simulation also decreases with the solvent polarity (Fig. 3.5b). These observations indicate that the formation of ion pairs could be modulated by solvent polarity. This is

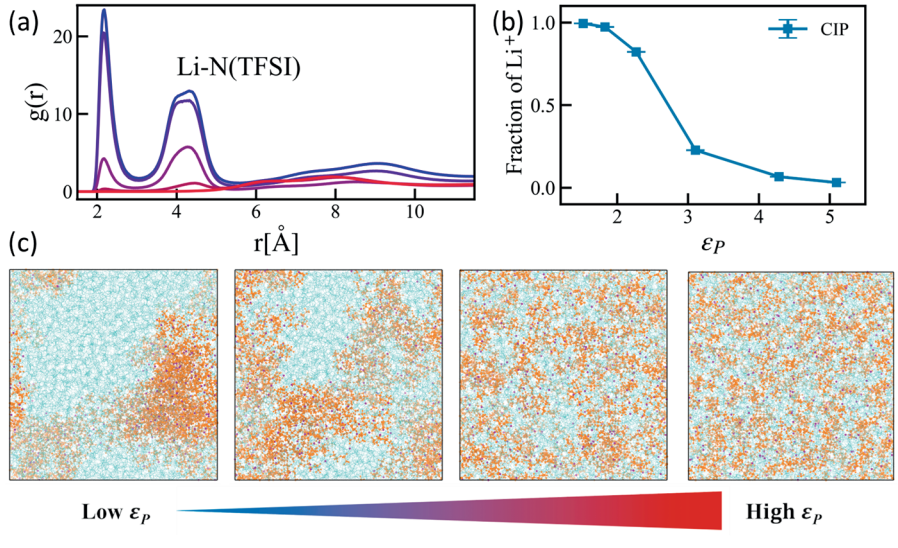

Figure 3.5: (a) The Li−N(TFSI) radial distribution functions g(r) at different solvent polarity strengths. (b)The fraction of Li^+ as a function of solvent polarity. (c) Modulation of ion pairing in PEO-LiTFSI systems by solvent polarity ε_p. Sky blue - PEO chains, Purple - Li ions, Orange - TFSI ions. Color map: Blue to red – low to high ε_p. Adapted with permission from [125] Copyright 2022 American Chemical Society.

also displayed in Fig. 3.5c, where the different distribution of ion pairs was observed at different solvent polarities.

3.2.2 Ion-pairing vs. cation-anion distinct ionic conductivity

The lifetime of ion pairs τ_{+-} were extracted from the normalized time correlation function of the cation-anion pairs that lies within a given cut-off distance and a time period. A detailed description of the methods to calculate lifetime can be found in **Paper II**. From Fig. 3.6a, the lifetime of ion pairs increases when ε_p is either high or low, and it reaches a minimum at the

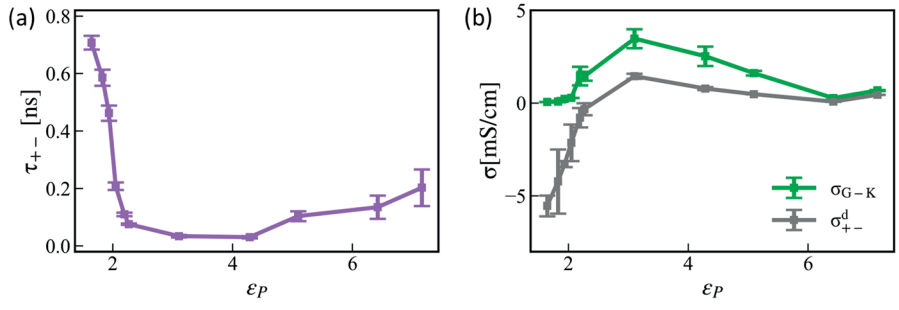

Figure 3.6: (a) The lifetime of ion pairs τ_{+-} computed from the SSP method (see Eq. 2-4 in **Paper II**) as a function of ε_p (a) The total conductivity σ_{G-K} computed from the Green−Kubo relation and the cation−anion distinct conductivity σ^d_{+-} as a function of ε_p.

intermediate value of ε_p. The total Green−Kubo conductivity σ_{G-K} as a function of solvent polarity is shown in Fig. 3.6b, follows a similar trend as the diffusion coefficients in **Paper I** and agrees with other recent studies of polymer electrolyte systems.[63] The effect of ion pairing on the ionic conductivity can be assessed from the cation-anion distinct ionic conductivity σ^d_{+-} or its equivalent Onsager transport coefficients Ω_{+-}. Note that $\sigma^d_{+-} > 0$ corresponds to anticorrelated cation−anion movements for the sign convention used in this work.

From Fig. 3.6a, b, one may attempt to relate the opposite trend in the total ionic conductivity σ_{G-K} to that of τ_{+-}. However, the observed increase in the lifetime at a lower dielectric constant regime ($\varepsilon_p < 2.3$) is much more rapid than at a higher dielectric constant regime ($\varepsilon_p > 3$). This suggests that there are different types of ion pairs in these polymer electrolyte systems. One can observe that the cation−anion distinct conductivity σ^d_{+-} goes from positive to negative when ε_p becomes smaller, i.e., from anticorrelated to correlated cation-anion motion.

In particular, the rapid decrement in σ^d_{+-} at lower ε_p seems to be in accordance with the rapid increment in τ_{+-} which shows that these two fundamental properties are closely related and plotted in Fig. 3.7. From this

figure, there exist two distinct regimes: σ^d_{+-} scales with $1/\tau_{+-}$ (for higher values of ε_p), and σ^d_{+-}scales with τ_{+-} (for lower values of ε_p). This observation could lead to a general scaling relation between these two properties for polymer electrolyte systems, i.e., $\sigma^d_{+-} = (A/\tau_{+-} + B\tau_{+-})$ where A and B are system-dependent coefficients.

The inverse relation is reminiscent of the Walden rule or the

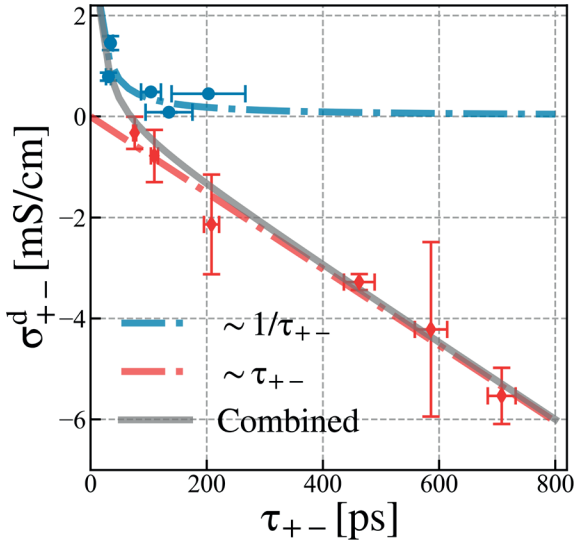

Figure 3.7: Scaling relation between the cation−anion distinct conductivity σ^d_{+-} and the lifetime of ion pairs τ_{+-} for PEO-LiTFSI polymer electrolyte systems with different solvent polarity strengths. Reproduced with permission from [125] Copyright 2022 American Chemical Society.

Stokes−Einstein relation, generally observed in ionic liquids, organic electrolytes, and salt-doped homopolymers.[68,117,118] The linear scaling relation is a signature of longer-lived ion pairs that reduce the total ionic conductivity. Therefore, what matters to discussions of the ion-pairing effect on transport properties in polymer electrolytes is not whether ion pairs are present or not in the system, but rather how long they live.

3.3 Relationship between ionic transport and ion-ion correlations

In **Paper III**, the relationship between the cation transference number and the ion-ion correlations was explored. In recent studies for a typical polymer electrolyte system, i.e., PEO−LiTFSI, a negative transference number was reported with Newman's approach[47,48], which implies that cations were being transported to the positive electrode. This instigated a series of experimental and computational works to understand its molecular origins. While the formation of ion aggregates (negatively charged ion clusters) has often been suggested to cause such a phenomenon, only marginally negative values were observed in MD simulations[67,68], even when the correlation due to charged ion clusters was considered explicitly. However, the importance of the reference frame (RF) was overlooked in these studies while the transport coefficients are defined in different RF for different measurements.

3.3.1 Different reference frames

The cation transference number measured in these experiments is defined typically in the solvent-fixed RF (t_+^0). In a solvent-fixed RF, the transport properties are calculated relative to the solvent motion, i.e., the overall flux of solvent is 0. However, for the transference number as computed in MD simulations, the correlation functions are under the barycentric RF (t_+^M) (see Fig. 3.8). In a barycentric RF, the transport properties are calculated relative to a fixed point, either the origin or corner of a simulation box. This difference

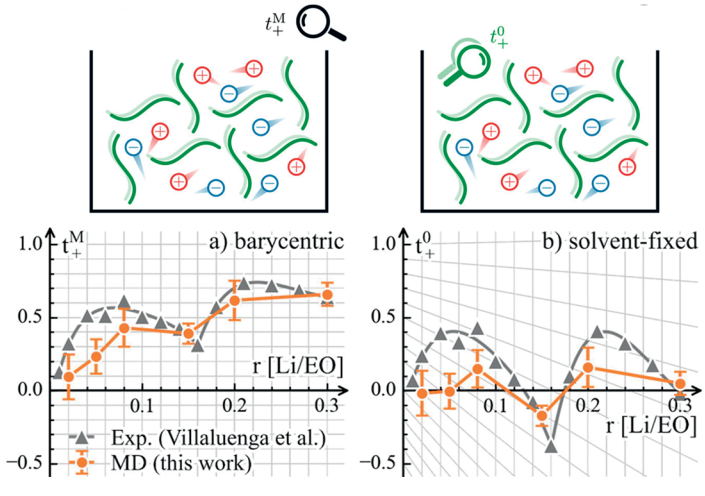

Figure 3.8: Schematic representations and transference number under (a) barycentric RF and (b) solvent-fixed RF in PEO−LiTFSI for different concentrations r [Li/ EO]. The experimental data and fitting of t_+^0 are reproduced from Ref. [48]. Adapted with permission from [69] Copyright 2022 American Chemical Society.

creates a conceptual gap when comparing experiments and simulations. A simple transformation rule between t_+^0 and t_+^M was proposed by Woolf and Harris[119]: $\omega_0 t_+^0 = t_+^M - \omega_-$, where ω_0 and ω_- are the mass fractions of solvent (polymer) and anion, respectively.

These transformations were applied to the transference numbers from Ref. [48] and compared with MD simulations in **Paper III** and shown in Fig. 3.8. The negative t_+ from the experiments could then be reproduced from MD simulations when transformed to the solvent-fixed RF. However, at this concentration t_+^M is still positive from both measurements. Due to the dependence of ω_- on t_+^0, at higher concentrations, it will become increasingly sensitive and shifts toward a downward trend. To understand this negative t_+^0, the RF dependence on ion-ion correlations was also studied.

3.3.2 Ion-ion correlations

The total ionic conductivity and different ion-ion correlations calculated from Onsager coefficients at both the RFs are plotted in Fig. 3.9. MD simulations consistently show a good agreement with the observed trends in the

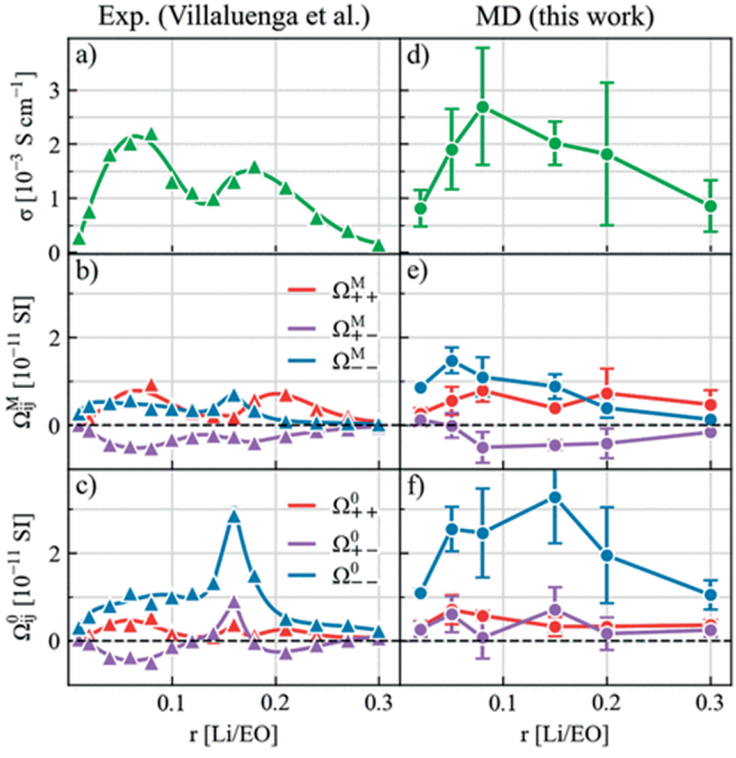

Figure 3.9: Ionic conductivity and Onsager coefficients under the barycentric and solvent-fixed RF derived from (a–c) experimental measurements and (d–f) MD simulations. The experimental measurements (▲) and fittings (curved lines) are converted from Ref. [48]. Reprinted with permission from [69] Copyright 2022 American Chemical Society.

experiments. This suggests that the ion-ion correlations were accurately captured in the MD simulations. From these trends, one can observe that Ω_{--} and Ω_{+-} are significantly affected upon the RF transformation as compared to Ω_{++}. At the concentration r=0.15 (negative t_+^0), the observed trends in $\Omega_{ij}$are $\Omega_{--}^0 > \Omega_{+-}^0 > \Omega_{++}^0 > 0$ and $\Omega_{--}^M > \Omega_{++}^M > 0 > \Omega_{+-}^M$, and in particular Ω_{+-} changes sign from negative to positive when converting from barycentric to solvent fixed RFs. To understand this change in sign, the cation-anion displacement correlations for the reference frames at this concentration are plotted in Fig. 3.10.

In the barycentric RF, anticorrelations between the displacements of cations and anions are observed, whereas these displacements are correlated

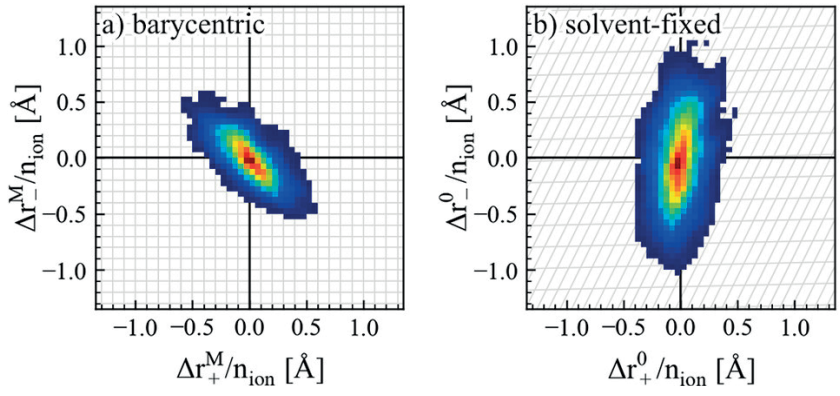

Figure 3.10: The correlations between mean displacements of cations (+) and anions (-) in barycentric RF (a) and solvent fixed RF (b). Reprinted with permission from [69] Copyright 2022 American Chemical Society.

for solvent-fixed RF. Since the transference numbers are directly dependent on $\Omega_{++} - \Omega_{+-}$, the negative cation-anion correlations give a positive t_+^M, and the positive correlations could lead to a negative t_+^0. The dependence of Ω_{+-}, Ω_{--}, and ω_- on t_+^0 indicates that the anions play a significant role in the Li-ion transference number, not only by its relative motion to the cation.

3.4 Relationship between coordination and ionic transport mechanisms

The ion transport mechanisms briefly studied in **Paper I** were categorized based on the cation-polymer coordination changes which are commonly found in the literature.[37–39,49] However, following the previous discussions in **Paper II** and **III**, the balanced interactions between polymer, cation, and anion are clearly relevant to the study the Li-ion transport, and especially at higher concentrations, anion-cation interactions cannot be neglected. So, in **Paper IV**, Li-ion transport mechanisms at different molecular weights and different salt concentrations (polymer-in-salt regime) are studied. Moreover, along with PEO, a carbonyl-based polymer, i.e., poly(ε-caprolactone) (PCL), is also studied to understand the dependence of functional groups on coordination and ion transport.[120–122] The information of the different systems studied can be found in Table 1 of **Paper IV**. As stated in the introduction, three main categories are considered: ion hopping, continuous motion and vehicular transport. Depending on the dominant coordination species, the transport mechanisms were then further classified into polymer-mediated and anion-mediated transport.

3.4.1 Coordination and Li-ion transport

The differences between the two polymer hosts in terms of the coordination of Li^+ to polymer backbone can be observed in Fig. 3.11a, b. As expected, with an increase in salt concentration, Li^+ coordination changes predominantly from polymer to anion. However, the total CN in PCL is lower than in PEO systems, possibly since the coordinating O atoms are less accessible in PCL due to steric effects. In Fig. 3.11c, similar trends in Li^+ diffusion coefficients can be observed for both PEO and PCL at different molecular weights and concentrations, i.e., the conductivity decrease with increasing molecular weight and salt concentration. Such similarities can be expected as both PEO and PCL have been low T_g polymers, and their flexibility affects the ion conduction.[121] High molecular weight and physical cross-links from the ions will thereby contribute to a lower segmental mobility. However, these similarities between the polymers are not reflected in the apparent cation transference numbers (t_+^{app}), as seen in Fig. 3.11d. Generally, a high concentration seems to promote high t_+^{app}, but with some exceptions for PCL. A higher M_n seems to promote a high t_+^{app} for PCL, but only for high concentrations, while rather the opposite is seen for PEO. The differences in these trends could arise from changes in transport mechanisms.

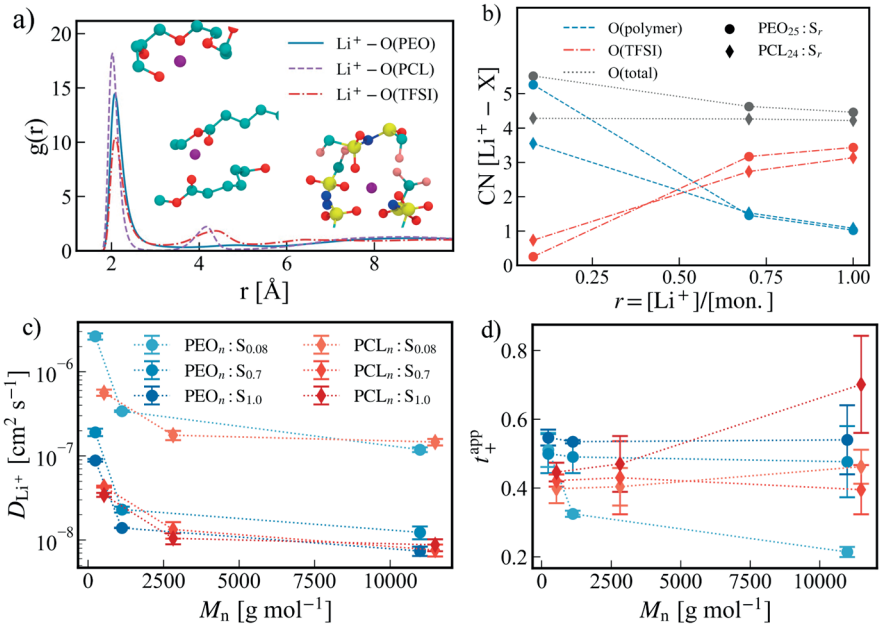

Figure 3.11: a) Radial distribution functions $g(r)$ for Li^+ with O atoms from the polymer backbone and O atoms form TFSI for PEO_{25}:$S_{0.7}$ and PCL_{24}:$S_{0.7}$ systems along with their representative local coordination. Li^+: purple, O: red, C: cyan, N: blue, S: yellow, and F: pink. b) The coordination numbers (CN) of Li^+ – O(polymer), Li^+ – O(TFSI) and Li^+ – O(total) in the first coordination shell (first minimum in $g(r)$) as function of concentration for PEO_{25} and PCL_{24} systems. c) The Li^+ self-diffusion coefficients (D_{Li^+}) and d) apparent cation transference number (t_+^{app}) as function of polymer molecular weights (M_n) for both polymers at different concentrations.

3.4.2 Ion transport mechanisms

While the $g(r)$ and CN only provide a static picture of local coordination environments, the ion transport mechanisms can be estimated by analyzing the evolution of these environments. The above defined modes of transport (hopping, continuous, vehicular) can be further categorized depending on the dominant ligand species (mediated mobility) and on which coordinating species that remain in the coordination sphere (assisted mobility). A detailed description of these categorizations can be found in **Paper IV**.

In Fig. 3.12b, the estimated probability of each transport mechanism is plotted for PEO and PCL systems for the lowest concentration. It appears that the dominating transport mechanism for PEO and PCL are polymer-mediated continuous and vehicular modes, respectively, irrespective of the molecular weights. However, as seen in Fig. 5 and 6 in **Paper IV,** these mechanisms are highly sensitive to the applied cut-off distances (Δr) and time steps (Δt), which therefore needed to be carefully chosen. The low Δt used in Fig. 3.12b

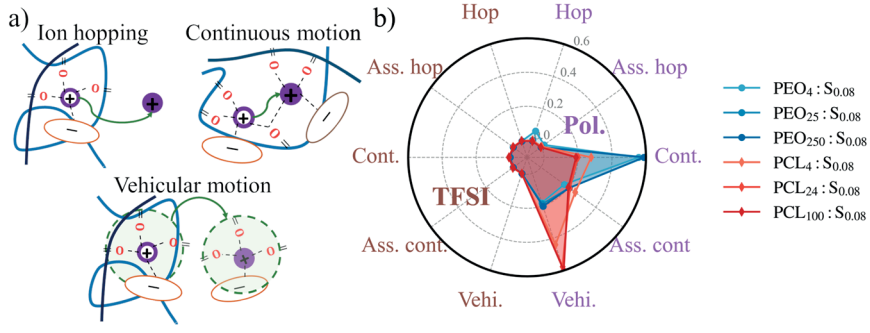

Figure 3.12: a) Schematic description of the three ion transport mechanisms: i) ion hopping - complete change of coordination; ii) continuous - partial change of coordination; and iii) vehicular - no change of coordination. Colors: blue and dark blue lines – different polymer chains; red – O atoms; purple – cation; orange and brown ovals – different anions; green arrow – motion of cation. b) Probability of type of ion transport mechanisms for both polymers at different molecular weights with salt concentration 0.08 i.e., $PEO_n{:}S_{0.08}$ and $PCL_n{:}S_{0.08}$. Here, Δt = 0.1 ns.

explains the overestimation of vehicular transport. However, it is most striking that no real hopping is seen in either system, which seems to be a true effect.

The t_+^{app} is plotted along with probabilities of different modes for all investigated systems in Fig. 3.13, as it could potentially give insight into the trends observed in Figure 3.11d. At low salt concentrations (Fig. 3.13a, b), continuous mobility is the dominating mechanism. Here, polymer-mediated transport is evident for both polymers which specifically is anion-assisted in PCL. The decrease seen in t_+^{app} for PEO as a function of M_n is correlated with an increase in the anion dynamics during the continuous transport mode. Also, at higher salt concentrations (r = 0.7 and 1.0), continuous mobility is dominating. Both polymer- and anion-mediated transport modes can be observed in Figure 3.13c, e for PEO and Figure 3.13d, f for PCL. When the salt concentration is further increased to r = 1.0, the distribution of transport modes is similar for the PEO systems as compared to r = 0.7 (Fig. 3.13c, e). However, an increase in the anion-mediated continuous mode can be noted, which is correlated with an increase in cation transference numbers at the highest salt concentration.

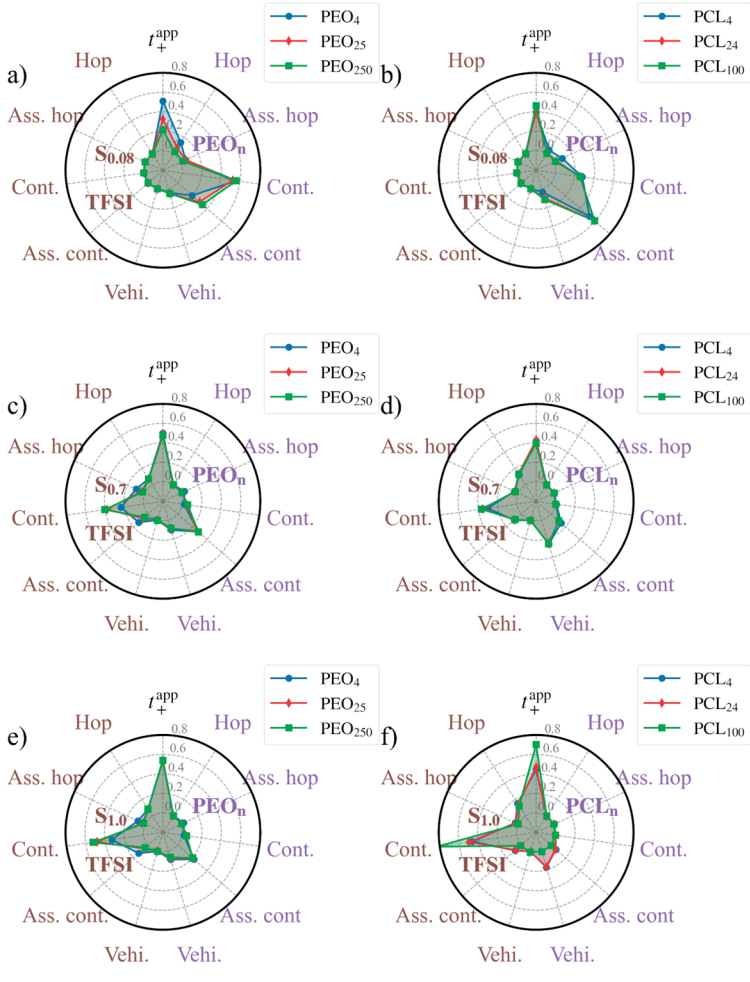

Figure 3.13: Probability of type of ion transport mechanisms and apparent cation transference number (t_+^{app}) as a function of molecular weight for both the polymers PEO (a, c, e) and PCL (b, d, f) at different salt concentrations with time step Δt of 1 ns and effective distance criterion Δr of 3 Å. The mechanisms are further categorized into the polymer- (purple; right) and anion- mediated (brown; left) ion transport.

In the PCL systems at the highest salt concentration and the highest M_n (Fig. 3.13f), the polymer-mediated transport is essentially absent, suggesting that the ion transport is fully decoupled from the polymer segmental motion, forming a PISE material. In the PISE regime, ion transport is reported to be similar to ion transport in ionic liquids, which agrees well with the data in Figure 8f. The formation of a PISE regime in PCL as compared to PEO is likely associated with the weaker ion coordination in PCL.

For the high-salt-concentration PCL system, the transference number also drastically increases with molecular weight, which was not observed in the other systems. As also noted for PEO, a high t_+^{app} at high salt concentrations

seems to be correlated with a high degree of anion-mediated continuous motion. This correlation may be related to the different Li^+ residence times (see Fig. 7 in **Paper IV**) with polymer and anion, suggesting that the ion transport is coupled to both the polymer and the anion motion.

3.5 Relationship between coordination strength and ionic transport

In contrast to **Papers I-IV**, **Paper V** focus on the importance of coordination strength between the cation and its ligands on the transport properties. To this end, three different carbonyl-containing polymer electrolyte systems at the same molecular weight and concentration were considered. Moreover, the investigated polyketone, polyester, and polycarbonate SPEs only differ in the functional groups by the presence of extra alkoxy oxygens in the polymer backbone (see Fig. 3.14a), thereby rendering a straight-forward comparison possible.

In Fig. 3.14b, when comparing the polyester (PCL) and polycarbonate (PTeMC) systems, the experimental ionic conductivity of PCL is always one order of magnitude higher than PTeMC. This could be explained by the higher T_g of the polycarbonate, indicating restriction in segmental motion. On the other hand, the polyketone (POHM) has a similar conductivity as PTeMC even though a very high experimental T_g was observed – but in turn coupled to a high degree of crystallinity. This can explain the Arrhenius-type behaviour observed for the conductivity of POHM (see Fig. 3 in **Paper V**), which indicates that ion transport is decoupled from the segmental motion of

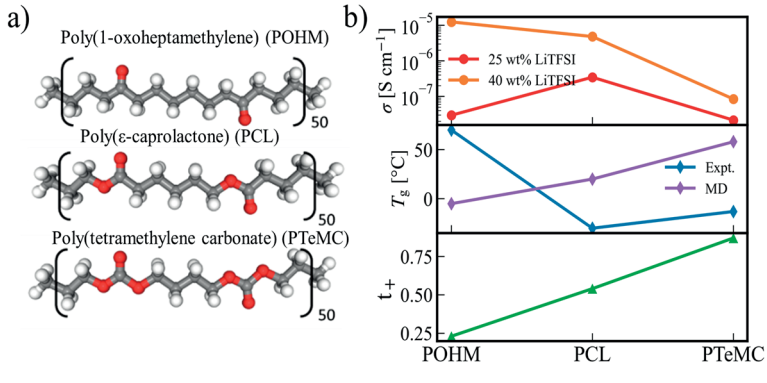

Figure 3.14: a) Polymer structures with the specific repeating units of the polyketone poly(1-oxoheptamethylene) (POHM, top), polyester poly(ε-caprolactone) (PCL, middle) and polycarbonate poly(tetramethylene carbonate) (PTeMC, bottom). b) Experimental total ionic conductivity at room temperature with 25 and 40 wt% LiTFSI (top), experimental and computational glass transition temperature (middle) and experimental cation transference number (bottom) for the three polymer electrolyte systems.

the polymer. However, from the MD simulations – where only the amorphous phases exists – the POHM has the lowest T_g, which was also observed experimentally when the salt content increased from 25 to 40 wt% LiTFSI (see Table 1 in **Paper V**). This suggests that the total ionic conductivity when the polymer is fully amorphous, is primarily dependent on the T_g of the polymers and thereby its segmental mobility. To understand the trends in the transference numbers (t_+) (Fig. 3.14b) from the experiments, further investigation of the coordination properties is needed.

3.5.1 Coordination environments

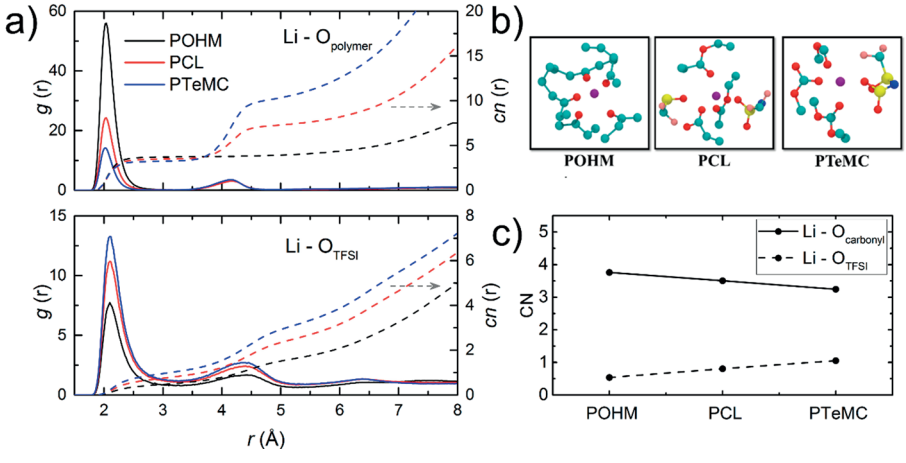

Figure 3.15: (a) Radial distribution functions $g(r)$ and coordination number functions $cn(r)$ for Li^+ with O atoms from the polymer backbone and TFSI for the three polymer electrolyte systems. (b) MD snapshots of Li^+ coordination environments within 5 Å for POHM (left), PCL (middle), and PTeMC (right). Li^+: purple, O: red, C: cyan, N: blue, S: yellow, and F: pink. (c) Coordination numbers (CN) in the first coordination shell of Li–O(carbonyl) and Li–O(TFSI) for the three polymer electrolyte systems.

The coordination between the Li^+ and carbonyl oxygens can be observed from the first peak in *g(r)* of $Li - O_{polymer}$ in Fig. 3.15a, while the second peak in PCL and PTeMC corresponds to the non-coordinating alkoxy oxygens in the polymer main chain. These observations are further confirmed from the snapshots in Fig. 3.15b. From the CNs for $Li - O_{polymer}$ and $Li - O_{TFSI}$ in Fig. 3.15b, Li^+ in POHM seems to coordinate mostly with polymer, then follows PCL and PTMC, while anion coordination to Li^+ follows the opposite trend, i.e., PTeMC > PCL > POHM. This suggests that POHM has a better solvating ability for LiTFSI as compared to the other polymers. However, the total CNs seem to be invariant to the extra O atoms in the polymer chain, which is

expected as the main coordinating group is the same for all polymer systems, i.e., the carbonyl oxygen.

3.5.2 Coordination strengths

The binding strength is a key property in coordination chemistry, with a direct influence on the local solvation structure and the resulting transport properties of the system. To estimate these strengths, binding energies (BE) of Li^+ in all the three polymer electrolytes systems were calculated and are plotted in Fig. 3.16. The BE (System – Li) estimates the BE of Li^+ with both polymer and salt taken into account. Interestingly, this value is almost the same for the three polymers. However, BE (Polymer – Li) can be seen to decrease from POHM to PCL and PTeMC, which shows that the coordination strength of Li^+ to the polymer decreases with the extra alkoxy oxygens. This also seem to lead to a higher t_+ in PCL and PTeMC, which one could expect – a less tightly bonded

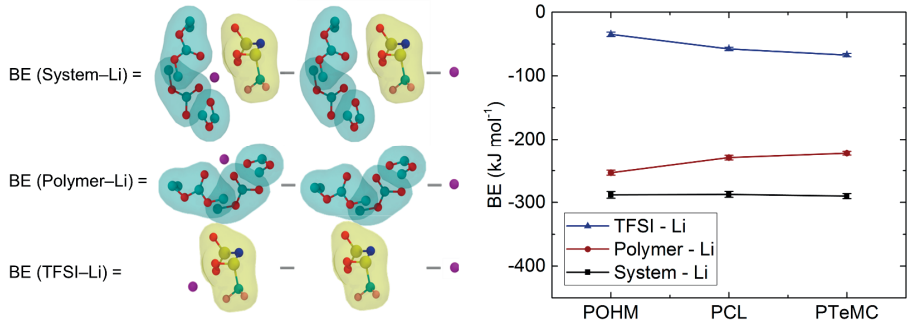

Figure 3.16: The average binding energy (BE) of all Li^+ in the simulations with both polymer and TFSI [System–Li], as well as just with polymer [Polymer–Li] and TFSI [TFSI–Li]. On the left are schematic representations of these terms. Surface colors: cyan (polymer backbone) and yellow (TFSI molecules).

cation can move more easily out of its coordination sphere. Furthermore, one can observe that the BE and CN follow similar trends irrespective of the coordination species. This suggests that the difference in interaction strength between Li^+ and polymer could be an effect of the different number of coordinating groups (which is highest for POHM), rather than the strength of the individual interactions.

Therefore, the electrostatic energy of Li^+ with the carbonyl group in the three systems was calculated to separate the effects from coordination numbers and strengths. However, these values follow a similar trend as that observed for the BE values (Polymer – Li); i.e., Li^+ binds most strongly with the polyketone and then to polyester and polycarbonate. This difference correlates well to the change in the electronic density on the carbonyl group

(see Table 2 in **Paper V**), which in turn affects the structural rigidity of the polymer backbone.

The polyketones – a very unexplored category of SPE materials – thus seem to be a promising SPE candidate as they show high conductivity (at room temperate) and potentially low T_g but are somewhat limited a strong cation coordination to the backbone (leading to a reduced t_+) and a high degree of crystallinity. On the other hand, polycarbonates are weekly coordinated by Li^+ and thereby promote high cationic currents but are in turn limited by their low ionic conductivity due to their high T_g. As expected, the polyesters constitute somewhat of an intermediate of those other two polymers, both in terms of structural and transport properties.

4. Conclusions

Understanding the complex ion transport phenomenon in solid polymer electrolytes (SPEs) is crucial for enhancing the total ionic conductivity in SPE-based LIB. In this thesis, all-atom MD simulations provide insights into the various factors that affect the ion and polymer structure-dynamic relations and to understand the conceptual gaps between experimental and computational studies, including solvent polarity, ion-pairing, ion-ion correlation, molecular weight, and salt concentration.

The solvent polarity was investigated by scaling the charges on the polymer backbone in MD simulations of PEO-LiTFSI systems (**Paper I**). In doing so, the glass transition temperature was also found to be directly dependent on the polarity. These two factors were separated by choosing a normalized temperature so that observed transport properties relied solely on solvent polarity. A maximum in the Li-ion diffusion coefficient with respect to ε_p was then observed. It was attributed to balanced interactions between Li-ions with anions and polymers that lead to more frequent inter-segmental motions. Since the solvent polarity also modulates the formation of charge-neutral ion pairs, their contribution to total ionic conductivity was then studied in **Paper II**. At low solvent polarity, the ion pairs lived longer and contributed negatively to the total ionic conductivity. As the polarity increases, the cation-anion distinct conductivity is found to change its sign to positive where the ion pairs are shorter-lived. A scaling relation between these two parameters was then established, which could use to estimate the ion pair lifetime experimentally. This showed the importance of ion-pair lifetime when discussing their contribution to total ionic conductivity.

To establish a thorough comparison between experiment and simulation for the PEO-LiTFSI system, the Onsager transport coefficients were computed in **Paper III**. The experimentally observed negative transference numbers were able to reproduce from MD simulation using a solvent-fixed reference frame. A good agreement in the transference numbers and the Onsager coefficients was found with a proper transformation between the experimental measurements and MD simulations. This shows that while studying the ion−ion correlations, one must ensure the same reference frame during the discussion.

Going beyond the polyether-based system, a detailed analysis of the ion transport mechanisms was made by comparing MD simulations of PEO and

PCL systems (**Paper IV**). By tracking the cation coordination changes, three transport mechanisms were categorized and quantified, i.e., ion hopping, continuous (successive change of coordination), and vehicular modes. In both systems, ion hopping was essentially absent, as can be expected in systems with strong ion–polymer interactions. Furthermore, a higher influence of polymer-mediated vehicular transport was observed in PCL systems than in PEO systems, and a correlation was found between the anion-mediated continuous motion and the apparent transference numbers, irrespective of polymer and salt concentrations.

Following the same line, three different types of carbonyl-coordinating polymers were compared: polycarbonates, polyesters, and polyketones (**Paper V**). As revealed by experimental measurements as well as molecular dynamics simulations, the polyketone possesses the lowest glass transition temperature, but the ion transport is limited by a high degree of crystallinity. The polycarbonate, on the other hand, displays a relatively low coordination strength but is instead limited by its low molecular flexibility. Finally, the polyester generally performs as an intermediate between the other two, which is reasonable when considering its structural relation to the alternatives. On the other hand, the study show a great potential for the polyketone systems, which have so far not been thoroughly explored for SPEs.

Overall, the series of works presented in this thesis demonstrates that MD simulation remains a highly useful tool to shed light on the molecular mechanism of ion transport in SPEs, and will certainly be critical also in future in-depth studies of SPE systems. However, it is also apparent that cares need to be taken when comparing MD simulation and experiment results, because different conditions may apply in these two cases. Despite that the main technique of molecular modeling in this thesis is classical all-atom MD simulation, future work on multi-scaling modeling of SPEs, as outlined in the introduction, is the direction to go to obtain a more profound knowledge and understand the functionality of SPEs in battery devices. For example, the use of coarse-grained simulation would be desirable for studying block co-polymer systems that could satisfy the need for both mechanical and transport properties. By expanding the methodological portfolio beyond MD, a larger range of properties can be scrutinized, and their interplay understood. This would render a computational tool that can be used for molecular design, in order to create SPEs with the desired properties. This thesis can hopefully serve as a starting point by highlighting some very important molecular-level properties and their interdependence.

5. Popular scientific summary

5.1 Summary in English

Since Sony commercialized lithium-ion batteries (LIB) in 1991, they have become an essential commodity in the day-to-day life of society. The impact of LIBs in real life, from energy banks to cell phones, cameras, electric vehicles, and many more applications, has been recognized by the Nobel Prize in 2019, the most prestigious scientific award. Electric vehicles are known to be more sustainable than their conventional counterparts with flammable fuel. However, LIBs are not 100% safe, as seen by multiple battery explosions in for example Samsung phones and Tesla cars. With their tremendous growth in battery manufacturing, even a tiny percentage of malfunctioning cells could scale up to a huge number of accidents.

An LIB comprises three main components, i.e., a positive electrode, an electrolyte, and a negative electrode. In the electrodes, the current is conducted as electrons; in the electrolyte, it is through the transport of ions (lithium ions). The main reason behind these safety issues is the use of liquid electrolytes in almost all commercial LIBs. These liquid electrolytes consist of lithium salts dissolved in organic solvents that are highly flammable. Using liquid electrolytes is also associated with possible short circuit that could ignite the fire. One way to address these safety problems is to replace the liquid electrolytes with solid counterparts, e.g., solid polymer electrolytes (SPEs).

An SPE is generally defined as a solvent-free electrolyte with dissolved Li-salt in a polymer host material that conducts these ions. When the salt is completely dissolved, primarily the oxygen atoms in the polymer will bind with lithium-ion and form what is called a coordination shell. The ion transport occurs by breaking and forming these bonds, i.e., by changing its coordination shells. Since the polymers are much bulkier than liquid electrolytes, the total ion transport is limited due to slower polymer motion. However, to improve this transport, which is necessary for operating the battery, one has to understand the ion transport mechanisms in SPEs thoroughly and which properties that effects it. To contribute to this field is the main goal of this thesis.

Since these motions occur at the atomistic level, molecular dynamics (MD) simulations have here been used to study the ion transport. In MD simulations, atoms are modeled as hard balls, and a set of equations and parameters governs the interactions between these balls. After running the simulation in a

computer, a movie of how these balls move is recorded, and by analyzing these motions, one can calculate different ion transport properties and what properties that control them. Different structure-transport property relationships were thereby explored using MD simulations.

In **Paper I**, the effect of solvent polarity on ion transport was investigated for a polyether-based SPE; the most common SPE material. The polarity of a solvent or polymer measures how well it can separate the salt into cations (positive charge) and anions (negative charge). My simulations show that fast ion transport was observed when the polarity is not too high or too low. The interactions between cation, anion, and polymer were found to be optimum at the intermediate polarity. If the polymer cannot separate cations and anions, they will combine and form a charge-neutral ion pair, which will not help to conduct ions. Since all the ions are continuously moving, these pairs will constantly break and form, and the time taken to break these pairs is known as ion pair lifetime. The importance of ion pair lifetime in SPEs was investigated in **Paper II**. If this ion pair lifetime is short, these pairs will actually help improving the total ion conduction as they break and form more frequently. But if the ion pairs lived longer, they contribute negatively to the total ion transport. Since these events happen at a very small time scale, i.e., 10^{-11} to 10^{-9} seconds, it is difficult to calculate this in experiments; however, it is possible to calculate the contribution of ion pair transport through computer simulations. The ion pair lifetime can be estimated in experiments using the relation presented in **Paper II**.

In recent experiments, the lithium ions in SPE and other materials has been found to sometimes travel in the opposite direction in the battery, i.e., towards the positive electrode (cathode). This has so far been challenging to model in computational studies. However, the ion transport direction depends on where you observe, also known as the reference frame. Experimental and computational studies often use different reference frames, but this difference is often overlooked. In **Paper III**, it was found that when observed through the same reference frame, both experiments and MD simulations actually see the same direction of ion transport. So one has to remember when comparing different studies, that the reference frame should be kept the same.

Paper IV compared ion transport mechanisms in polyether (as in Paper **I-III**) and with another type of polymer; a polyester with another chemical group (a carbonyl group) that is coordinating to the lithium ion. It was then found that when studying cation transport in SPEs, one must consider its coordination with both polymers and anions, and that the anions play a significant role in the ionic transport. Finally, in **Paper V**, three different carbonyl-containing polymers were compared: polyketones, polyesters, and polycarbonates. These three polymers are structurally similar, but differ by the number of oxygen atoms close to the carbonyl group. It was found that the binding strength of carbonyl oxygen to lithium decreases with extra oxygen

in the polymer. This leads to relatively more of cation transport, as these bonds to the polymer break more easily.

In summary, this thesis has shown that by performing MD simulations, one can gain insights into factors that affect the ion transport mechanisms in SPEs. Furthermore, this work also addresses some common pitfalls one can face when comparing experimental and computational studies.

5.2 Sammanfattning på svenska

Sedan Sony kommersialiserade litium-jonbatterier (LIB) år 1991 har de blivit en väsentlig komponent i samhällslivet. Påverkan från LIB i vardagen, vad gäller allt från energilager till mobiltelefoner, kameror, elektriska fordon, och många mer tillämpningar, uppmärksammades genom Nobelpriset 2019, den mest prestigefyllda vetenskapliga utmärkelsen. Elektriska fordon är mer hållbara än de konventionella som använder bränslen. Dock är inte batterierna i dem 100% säkra, vilket har setts genom flera LIB-relaterade explosioner i t ex Samsungs telefoner eller Tesla-bilar. Med en mycket stor tillväxt i batteriproduktionen så räcker det med att bara någon liten del av en procent av cellerna fungerar felaktigt, för att orsaka ett jättestort antal olyckor.

Ett LIB består huvudsakligen av tre komponenter: en positiv elektrod, en elektrolyt och en negativ elektrod. Den elektriska strömmen leds i form av elektroner i elektroderna, medan den leds via transport av joner (litiumjoner) i elektrolyten. Den huvudsakliga orsaken bakom säkerhetsproblemen i LIB är de flytande elektrolyterna som används. Dessa vätskebaserade elektrolyter består av litiumsalter som är lösta i brandfarliga organiska lösningsmedel. Användningen av flytande elektrolyter är också kopplat till möjliga kortslutningar i batteriet, vilket i sin tur kan orsaka branden. Ett sätt att överkomma dessa säkerhetsproblem är därmed att ersätta de flytande elektrolyterna med sådana i fast form, t ex, en polymerelektrolyt (förkortat SPE).

En SPE definieras oftast som en elektrolyt där en litiumsalt är löst i ett polymert värdmaterial fritt från flytande lösningsmedel, och som kan leda joner. När saltet löses upp är det främst till syreatomer i polymerkedjan som litiumjonen binder till, och som då bildar vad som kallas ett koordinationsskal. Jontransporten sker genom att bryta och bilda nya sådana bindningar, dvs genom att koordinationsskalet förändras. Men eftersom polymerer är större och trögare än molekylerna i flytande elektrolyter så blir den totala jontransporten begränsad, eftersom polymeren rör sig långsamt. För att förbättra denna jontransport, vilket är väsentligt för batteriets prestanda, måste en grundläggande förståelse skapas för mekanismerna bakom jontransport i SPE, och vilka egenskaper som påverkar dem. Att bidra till detta är målet med denna avhandling.

Sedan dessa rörelser sker på den atomära nivån har molekyldynamiksimuleringar (MD) använts här för att studera jontransporten. I MD-simuleringar modelleras atomer som hårda sfärer, och ett antal ekvationer och parametrar styr hur de interagerar. Efter att ha datorsimulerat hur systemet utvecklas med tid så skapas en filmsekvens av atomernas rörelsemönster, och genom att analysera detta så kan man beräkna olika jontransportegenskaper och vilka egenskaper som kontrollerar dem. Olika relationer mellan struktur- och transportegenskaper kunde därmed studeras med MD i den här avhandlingen.

I **Papper I** undersöktes effekten av lösningsmedelspolaritet för en polyeter-baserad SPE; det vanligast förekommande SPE-materialet. Polaritet hos ett lösningsmedel eller en polymer mäter hur väl det kan separera ett salt till katjoner (positivt laddade) och anjoner (negativt laddade). Mina simuleringar visar att snabb jontransport uppträder när polariteten inte är vare sig för hög eller för låg. Interaktionerna mellan katjon, anjon och polymer fanns vara optimal vid en intermediär polaritet. Om polymeren inte kan separera katjoner och anjoner så kommer de istället att bilda neutralt laddade jonpar, vilka ofta inte bidrar till jonledningen. Men sedan alla joner kontinuerligt är i rörelse kommer dock dessa jonpar brytas och återbildas, och tiden detta tar utgör jonparets så kallade livslängd. Vikten av livslängden hos jonpar i SPE studerades i **Papper II**. Om livslängden är kort visar det sig att dessa par faktiskt kommer att bidra till att förbättra jonledningsförmågan, då de bryts och återbildas mer frekvent. Men om jonparen istället lever längre kommer de att påverka negativt till jontransporten. Eftersom de här processerna sker på en mycket liten tidsskala, 10^{-11} till 10^{-9} sekunder, är det svårt att studera dessa experimentellt. Emellertid går det att beräkna bidragen från jonparstransport genom datorsimuleringar. Jonparens livstid går att uppskatta experimentellt genom att använda den beskrivning som presenteras i **Papper II.**

I experiment som gjorts under senare tid har det uppvisats att litiumjoner i SPE och andra material ibland kan färdas i motsatt riktning än vad som förväntas i batteriet, dvs mot det positiva elektroden (katoden). Detta har hittills visat sig svårt att reproducera i datormodeller. Riktningen av jontransport påverkas dock av varifrån den iakttas – det så kallade referenssystemet. Experimentella och datorbaserade studier använder ofta olika referenssystem, vilket inte sällan bortses från i dessa studier. I **Papper III** visades det att när jontransporten observeras från samma referenssystem så stämmer experiment och MD-simuleringar bättre överens avseende riktningen på jontransport. Man måste därmed ta hänsyn till referenssystemet när olika studier jämförs med varandra.

Papper IV i sin tur jämför jontransportmekanismer i polyetrar (som användes i **Papper I-III**) med en annan typ av polymer; en polyester med en annan kemisk typ av grupp (en karbonyl) som koordinerar till litiumjonen. Det sågs då att när man studerar transporten av katjoner i en SPE, så spelar anjonen en avgörande roll. Slutligen, i **Papper V**, jämfördes tre olika

karbonylinnehållande polymerer: polyketoner, polyestrar och polykarbonater. Dessa tre polymerer är strukturellt lika, men skiljer sig åt vad gäller antalet syreatomer som gränsar till karbonylgruppen. Det fanns då att bindningsstyrkan mellan karbonylgruppen och litium minskar med extra antal syren. Detta leder till att den relativa transporten av katjoner ökar, då dessa bindningar till polymeren bryts lättare.

Sammanfattningsvis visar denna avhandling att MD-simuleringar gör att man kan nå stora insikter kring vilka faktorer som styr jontransporten i SPE-material. Avhandlingen pekar också ut några fallgropar som kan förekomma när man jämför experimentella studier med datorsimuleringar.

6. Acknowledgements

First, I would like to sincerely thank my supervisors, Prof. Daniel Brandell, and Dr. Chao Zhang, for allowing me to perform research under your guidance. You have provided me the freedom to explore my research and monitored me with proper direction. Furthermore, you both have always been able to understand my problems and supported me professionally and personally. I am delighted that I could learn and nurture my knowledge from you guys. Second, Dr. Jonas Mindemark, I would like to thank you for the help, assistance, and guidance I have received from you throughout my Ph.D. You have improvised my knowledge in linking computational to real-world experiments. This was a great source of inspiration and experience for me.

Next, I would like to thank Yunqi, working with you was always so educational for me and thanks to all my co-authors for your valuable inputs. Then, I thank to all the past and present members in PUB and TEOROO groups, for the scientific and non-scientific discussions. Then, I would also like to thank all my colleagues in the department and administration for creating a pleasant working environment with welcome faces. Also, thanks to Dr. Luciano and group for hosting me in Brazil and Dr. Lisa Hall and group for research exchange in Ohio, I had great experience in working with you.

Moreover, I would like to express my sincere gratitude to Dr. R. S Swathi, my supervisor during my bachelor's and master's programs. Your lectures were my motivation and working with you inspired me to build a future in computational chemistry. Finally, my heartfelt thanks to Dr. Vennapusa Sivaranjana Reddy for the sincere support and trust that you have shown in me.

Athira, no words can express my gratitude towards you, but I hope my love speaks it. You are my smile, courage, confidence, breath, and life. I am happy when I am with you; you will always remain the strength behind all my success. Sorry for the stressful last few months, I will make it up when it’s your time. Amma, though you were not with me, a small part of you still lives in me. Thank you so much for being an idol in my childhood. I would also thank you for the unconditional love and support I received from my family.

Special thanks to my small family in Sweden. Jithin, Geethanjali, Alma, Akshay, Athira, Prabhakar, Anuja, Vishnu, Gautham. Thanks a lot for being my family and creating many memorable moments together. Also, special

thanks to Gopi, Saritha, Siya, Shourya, and Siddhi. You have completed my family here.

Finally, I would like to thank my laptop for surviving this long and also to computational resources from SNIC and funding from ERC.

7. References

1. Nishi, Y. Lithium ion secondary batteries; Past 10 years and the future. *Journal of Power Sources* **100**, 101–106 (2001).
2. Armand, M. & Tarascon, J.-M. Building better batteries. *Nature* **451**, 652–657 (2008).
3. Armand, M. *et al.* Lithium-ion batteries – Current state of the art and anticipated developments. *Journal of Power Sources* **479**, 228708 (2020).
4. Cano, Z. P. *et al.* Batteries and fuel cells for emerging electric vehicle markets. *Nature Energy* **3**, 279–289 (2018).
5. Bresser, D., Moretti, A., Varzi, A. & Passerini, S. The Role of Batteries for the Successful Transition to Renewable Energy Sources. in *Encyclopedia of Electrochemistry* 1–9 (Wiley, 2020). doi:10.1002/9783527610426.bard110024.
6. The Nobel Prize in Chemistry 2019 - NobelPrize.org. https://www.nobelprize.org/prizes/chemistry/2019/summary/.
7. Goodenough, J. B. & Park, K. S. The Li-ion rechargeable battery: A perspective. *J Am Chem Soc* **135**, 1167–1176 (2013).
8. Blomgren, G. E. The Development and Future of Lithium Ion Batteries. *Journal of The Electrochemical Society* **164**, A5019–A5025 (2017).
9. Armand, M. *et al.* Lithium-ion batteries – Current state of the art and anticipated developments. *Journal of Power Sources* **479**, 228708 (2020).
10. Samsung Galaxy Note 7 banned on all U.S. flights due to fire hazard. https://eu.usatoday.com/story/news/2016/10/14/dot-bans-samsung-galaxy-note-7-flights/92066322/.
11. Why the Fire that Incinerated a Tesla Was Such a Nightmare to Put Out | Live Science. https://www.livescience.com/62179-tesla-fire-cleanup-danger.html.
12. Perea, A., Dontigny, M. & Zaghib, K. Safety of solid-state Li metal battery: Solid polymer versus liquid electrolyte. *Journal of Power Sources* **359**, 182–185 (2017).
13. Wang, Q. *et al.* Thermal runaway caused fire and explosion of lithium ion battery. *Journal of Power Sources* **208**, 210–224 (2012).

14. Aurbach, D., Zinigrad, E., Teller, H. & Dan, P. Factors Which Limit the Cycle Life of Rechargeable Lithium (Metal) Batteries. *Journal of The Electrochemical Society* **147**, 1274 (2000).
15. Roth, E. P. & Orendorff, C. J. How electrolytes influence battery safety. *Electrochemical Society Interface* **21**, 45–49 (2012).
16. Wang, Q., Jiang, L., Yu, Y. & Sun, J. Progress of enhancing the safety of lithium ion battery from the electrolyte aspect. *Nano Energy* **55**, 93–114 (2019).
17. Xue, Z., He, D. & Xie, X. Poly(ethylene oxide)-based electrolytes for lithium-ion batteries. *Journal of Materials Chemistry A* **3**, 19218–19253 (2015).
18. Jana, A. & García, R. E. Lithium dendrite growth mechanisms in liquid electrolytes. *Nano Energy* **41**, 552–565 (2017).
19. Boaretto, N. *et al.* Lithium solid-state batteries: State-of-the-art and challenges for materials, interfaces and processing. *Journal of Power Sources* **502**, 229919 (2021).
20. Schnell, J. *et al.* All-solid-state lithium-ion and lithium metal batteries – paving the way to large-scale production. *Journal of Power Sources* **382**, 160–175 (2018).
21. Manthiram, A., Yu, X. & Wang, S. Lithium battery chemistries enabled by solid-state electrolytes. *Nature Reviews Materials* **2**, (2017).
22. Fergus, J. W. Ceramic and polymeric solid electrolytes for lithium-ion batteries. *Journal of Power Sources* **195**, 4554–4569 (2010).
23. Wang, S., Xu, H., Li, W., Dolocan, A. & Manthiram, A. Interfacial Chemistry in Solid-State Batteries: Formation of Interphase and Its Consequences. *J Am Chem Soc* **140**, 250–257 (2018).
24. Tan, S. J., Zeng, X. X., Ma, Q., Wu, X. W. & Guo, Y. G. Recent Advancements in Polymer-Based Composite Electrolytes for Rechargeable Lithium Batteries. *Electrochemical Energy Reviews* **1**, 113–138 (2018).
25. Brandell, D., Mindemark, J. & Hernández, G. *Polymer-based Solid State Batteries*. (De Gruyter, 2021). doi:10.1515/9781501521140.
26. Long, L., Wang, S., Xiao, M. & Meng, Y. Polymer electrolytes for lithium polymer batteries. *Journal of Materials Chemistry A* **4**, 10038–10069 (2016).
27. Fenton, D. E., Parker, J. M. & Wright, P. V. Complexes of alkali metal ions with poly(ethylene oxide). *Polymer (Guildf)* **14**, 589 (1973).
28. Wright, P. V. Polymer electrolytes - The early days. *Electrochimica Acta* **43**, 1137–1143 (1998).
29. Armand, M. Polymer solid electrolytes - an overview. *Solid State Ionics* **9–10**, 745–754 (1983).

30. Song, J. Y., Wang, Y. Y. & Wan, C. C. Review of gel-type polymer electrolytes for lithium-ion batteries. *Journal of Power Sources* **77**, 183–197 (1999).
31. Tigelaar, D. M., Meador, M. A. B. & Bennett, W. R. Composite electrolytes for lithium batteries: Ionic liquids in APTES cross-linked polymers. *Macromolecules* **40**, 4159–4164 (2007).
32. Liu, W. *et al.* Enhancing ionic conductivity in composite polymer electrolytes with well-aligned ceramic nanowires. *Nature Energy* **2**, 1–7 (2017).
33. Ahn, J. H., Wang, G. X., Liu, H. K. & Dou, S. X. Nanoparticle-dispersed PEO polymer electrolytes for Li batteries. *Journal of Power Sources* **119–121**, 422–426 (2003).
34. Mindemark, J., Lacey, M. J., Bowden, T. & Brandell, D. Beyond PEO—Alternative host materials for Li+-conducting solid polymer electrolytes. *Progress in Polymer Science* **81**, 114–143 (2018).
35. Arya, A. & Sharma, A. L. Polymer electrolytes for lithium ion batteries: a critical study. *Ionics (Kiel)* **23**, 497–540 (2017).
36. Doolittle, A. K. Studies in Newtonian Flow. II. The Dependence of the Viscosity of Liquids on Free-Space. *Journal of Applied Physics* **22**, 1471 (2004).
37. Borodin, O. & Smith, G. D. Mechanism of ion transport in amorphous poly(ethylene oxide)/ LiTFSI from molecular dynamics simulations. *Macromolecules* **39**, 1620–1629 (2006).
38. Maitra, A. & Heuer, A. Cation transport in polymer electrolytes: A microscopic approach. *Physical Review Letters* **98**, 1–4 (2007).
39. Diddens, D., Heuer, A. & Borodin, O. Understanding the lithium transport within a rouse-based model for a PEO/LiTFSI polymer electrolyte. *Macromolecules* **43**, 2028–2036 (2010).
40. Son, C. Y. & Wang, Z. G. Ion transport in small-molecule and polymer electrolytes. *Journal of Chemical Physics* **153**, (2020).
41. Wang, Y. *et al.* Decoupling of ionic transport from segmental relaxation in polymer electrolytes. *Physical Review Letters* **108**, (2012).
42. Bresser, D., Lyonnard, S., Iojoiu, C., Picard, L. & Passerini, S. Decoupling segmental relaxation and ionic conductivity for lithium-ion polymer electrolytes. *Molecular Systems Design and Engineering* **4**, 779–792 (2019).
43. Angell, C. A. Polymer electrolytes—Some principles, cautions, and new practices. *Electrochimica Acta* **250**, 368–375 (2017).
44. Kashyap, H. K., Annapureddy, H. V. R., Raineri, F. O. & Margulis, C. J. How is charge transport different in ionic liquids and electrolyte solutions? *Journal of Physical Chemistry B* **115**, 13212–13221 (2011).
45. Kirchner, B., Malberg, F., Firaha, D. S. & Hollóczki, O. Ion pairing in ionic liquids. *Journal of Physics Condensed Matter* **27**, 463002 (2015).

46. Shao, Y., Shigenobu, K., Watanabe, M. & Zhang, C. Role of Viscosity in Deviations from the Nernst−Einstein Relation. *J. Phys. Chem* **2020**, 4780 (2020).
47. Pesko, D. M. *et al.* Negative Transference Numbers in Poly(ethylene oxide)-Based Electrolytes. *Journal of The Electrochemical Society* **164**, E3569–E3575 (2017).
48. Villaluenga, I. *et al.* Negative Stefan-Maxwell Diffusion Coefficients and Complete Electrochemical Transport Characterization of Homopolymer and Block Copolymer Electrolytes. *Journal of The Electrochemical Society* **165**, A2766–A2773 (2018).
49. Devaux, D., Bouchet, R., Glé, D. & Denoyel, R. Mechanism of ion transport in PEO/LiTFSI complexes: Effect of temperature, molecular weight and end groups. *Solid State Ionics* **227**, 119–127 (2012).
50. Mindemark, J., Lacey, M. J., Bowden, T. & Brandell, D. Beyond PEO—Alternative host materials for Li+-conducting solid polymer electrolytes. *Progress in Polymer Science* **81**, 114–143 (2018).
51. Mishra, R., Baskaran, N., Ramakrishnan, P. A. & Rao, K. J. Lithium ion conduction in extreme polymer in salt regime. *Solid State Ionics* **112**, 261–273 (1998).
52. Borodin, O., Smith, G. D. & Henderson, W. Li+ cation environment, transport, and mechanical properties of the LiTFSI doped N-methyl-N-alkylpyrrolidinium+TFSI- Ionic liquids. *Journal of Physical Chemistry B* **110**, 16879–16886 (2006).
53. Zhang, H., Chen, F. & Carrasco, J. Nanoscale modelling of polymer electrolytes for rechargeable batteries. *Energy Storage Materials* **36**, 77–90 (2021).
54. Marchiori, C. F. N., Carvalho, R. P., Ebadi, M., Brandell, D. & Araujo, C. M. Understanding the Electrochemical Stability Window of Polymer Electrolytes in Solid-State Batteries from Atomic-Scale Modeling: The Role of Li-Ion Salts. *Chemistry of Materials* **32**, 7237–7246 (2020).
55. Nielsen, S. O., Bulo, R. E., Moore, P. B. & Ensing, B. Recent progress in adaptive multiscale molecular dynamics simulations of soft matter. *Physical Chemistry Chemical Physics* **12**, 12401–12414 (2010).
56. Tien, W. J. & Chiu, C. C. Generic parameters of trajectory-extending kinetic Monte Carlo for calculating diffusion coefficients. *AIP Advances* **8**, (2018).
57. Raihan, G. A., Shawon, M. A. S. & Saha, S. Numerical study of thermal and electrochemical behaviors of Lithium-ion battery for different cell chemistries using finite element method. *AIP Conference Proceedings* **2121**, 150006 (2019).
58. Liu, G. & Lu, W. A Model of Concurrent Lithium Dendrite Growth, SEI Growth, SEI Penetration and Regrowth. *Journal of The Electrochemical Society* **164**, A1826–A1833 (2017).

59. Grazioli, D., Zadin, V., Brandell, D. & Simone, A. Electrochemical-mechanical modeling of solid polymer electrolytes: Stress development and non-uniform electric current density in trench geometry microbatteries. *Electrochimica Acta* **296**, 1142–1162 (2019).
60. Franco, A. A. *et al.* Boosting Rechargeable Batteries R&D by Multiscale Modeling: Myth or Reality? *Chemical Reviews* **119**, 4569–4627 (2019).
61. Franco, A. A. Multiscale modelling and numerical simulation of rechargeable lithium ion batteries: Concepts, methods and challenges. *RSC Advances* **3**, 13027–13058 (2013).
62. Wheatle, B. K., Keith, J. R., Mogurampelly, S., Lynd, N. A. & Ganesan, V. Influence of Dielectric Constant on Ionic Transport in Polyether-Based Electrolytes. *ACS Macro Letters* **6**, 1362–1367 (2017).
63. Wheatle, B. K., Lynd, N. A. & Ganesan, V. Effect of Polymer Polarity on Ion Transport: A Competition between Ion Aggregation and Polymer Segmental Dynamics. *ACS Macro Letters* **7**, 1149–1154 (2018).
64. Wheatle, B. K., Fuentes, E. F., Lynd, N. A. & Ganesan, V. Influence of Host Polarity on Correlating Salt Concentration, Molecular Weight, and Molar Conductivity in Polymer Electrolytes. *ACS Macro Letters* **8**, 888–892 (2019).
65. Gutmann, V. Solvent effects on the reactivities of organometallic compounds. *Coordination Chemistry Reviews* **18**, 225–255 (1976).
66. Schauser, N. S. *et al.* The Role of Backbone Polarity on Aggregation and Conduction of Ions in Polymer Electrolytes. *J Am Chem Soc* **142**, 7055–7065 (2020).
67. France-Lanord, A. & Grossman, J. C. Correlations from Ion Pairing and the Nernst-Einstein Equation. *Physical Review Letters* **122**, 136001 (2019).
68. Fong, K. D., Self, J., McCloskey, B. D. & Persson, K. A. Onsager Transport Coefficients and Transference Numbers in Polyelectrolyte Solutions and Polymerized Ionic Liquids. *Macromolecules* **53**, 9503–9512 (2020).
69. Shao, Y., Gudla, H., Brandell, D. & Zhang, C. Transference Number in Polymer Electrolytes: Mind the Reference-Frame Gap. *J Am Chem Soc* **144**, 7583–7587 (2022).
70. Nitzan, A. & Ratner, M. A. Conduction in polymers. Dynamic disorder transport. *Journal of physical chemistry* **98**, 1765–1775 (1994).
71. Brooks, D. J., Merinov, B. v., Goddard, W. A., Kozinsky, B. & Mailoa, J. Atomistic Description of Ionic Diffusion in PEO–LiTFSI: Effect of Temperature, Molecular Weight, and Ionic Concentration. *Macromolecules* **51**, 8987–8995 (2018).

72. Webb, M. A. *et al.* Systematic computational and experimental investigation of lithium-ion transport mechanisms in polyester-based polymer electrolytes. *ACS Central Science* **1**, 198–205 (2015).
73. Rosenwinkel, M. P., Andersson, R., Mindemark, J. & Schönhoff, M. Coordination effects in polymer electrolytes: Fast Li+ transport by weak ion binding. *Journal of Physical Chemistry C* **124**, 23588–23596 (2020).
74. Eriksson, T., Mace, A., Mindemark, J. & Brandell, D. The role of coordination strength in solid polymer electrolytes: compositional dependence of transference numbers in the poly(ε-caprolactone)–poly(trimethylene carbonate) system. *Physical Chemistry Chemical Physics* **23**, 25550–25557 (2021).
75. Feynman, R. P., Leighton, R. B. & Sands, M. L. *The Feynman lectures on physics*. (Addison-Wesley Pub. Co., 1963).
76. Tuckerman, M. E. Ab initio molecular dynamics: Basic concepts, current trends and novel applications. *Journal of Physics Condensed Matter* **14**, (2002).
77. Chen, M. *et al.* Ab initio theory and modeling of water. *Proc Natl Acad Sci U S A* **114**, 10846–10851 (2017).
78. Heenen, H. H., Gauthier, J. A., Kristoffersen, H. H., Ludwig, T. & Chan, K. Solvation at metal/water interfaces: An ab initio molecular dynamics benchmark of common computational approaches. *Journal of Chemical Physics* **152**, 144703 (2020).
79. Paquet, E. & Viktor, H. L. Computational Methods for Ab Initio Molecular Dynamics. *Advances in Chemistry* **2018**, 1–14 (2018).
80. Boero, M., Parrinello, M., Weiss, H. & Hüffer, S. A first principles exploration of a variety of active surfaces and catalytic sites in Ziegler-Natta heterogeneous catalysis. *Journal of Physical Chemistry A* **105**, 5096–5105 (2001).
81. Cavalli, A., Carloni, P. & Recanatini, M. Target-related applications of first principles quantum chemical methods in drug design. *Chemical Reviews* **106**, 3497–3519 (2006).
82. Paul, W. & Smith, G. D. Structure and dynamics of amorphous polymers: Computer simulations compared to experiment and theory. *Reports on Progress in Physics* **67**, 1117–1185 (2004).
83. Karplus, M. & McCammon, J. A. Molecular dynamics simulations of biomolecules. *Nature Structural Biology* **9**, 646–652 (2002).
84. Hollingsworth, S. A. & Dror, R. O. Molecular Dynamics Simulation for All. *Neuron* **99**, 1129–1143 (2018).
85. Abraham, M. J.;van der Spoel, D.; Lindah, E.; Hess, B. ; and the G. devolpment team. GROMACS User Manual version 2018. *GROMACS User Manual version 2018* www.gromacs.org (2018).
86. Jensen, F. *Introduction to Computational Chemistry*. (Third Edit.; John Wiley & Sons, 2017).

87. Berendsen, H. J. C., Postma, J. P. M., van Gunsteren, W. F., Dinola, A. & Haak, J. R. Molecular dynamics with coupling to an external bath. *The Journal of Chemical Physics* **81**, 3684–3690 (1984).
88. Bussi, G., Donadio, D. & Parrinello, M. Canonical sampling through velocity rescaling. *Journal of Chemical Physics* **126**, 014101 (2007).
89. Andersen, H. C. Molecular dynamics simulations at constant pressure and/or temperature. *The Journal of Chemical Physics* **72**, 2384–2393 (1980).
90. Nosé, S. A molecular dynamics method for simulations in the canonical ensemble. *Molecular Physics* **52**, 255–268 (1984).
91. Hoover, W. G. Canonical dynamics: Equilibrium phase-space distributions. *Physical Review A* **31**, 1695–1697 (1985).
92. Parrinello, M. & Rahman, A. Polymorphic transitions in single crystals: A new molecular dynamics method. *Journal of Applied Physics* **52**, 7182–7190 (1981).
93. González, M. A. Force fields and molecular dynamics simulations. *École thématique de la Société Française de la Neutronique* **12**, 169–200 (2011).
94. Borodin, O. & Smith, G. D. Development of many-body polarizable force fields for Li-battery components: 1. Ether, alkane, and carbonate-based solvents. *Journal of Physical Chemistry B* **110**, 6279–6292 (2006).
95. Chen, X., Chen, F., Liu, M. S. & Forsyth, M. Polymer architecture effect on sodium ion transport in PSTFSI-based ionomers: A molecular dynamics study. *Solid State Ionics* **288**, 271–276 (2016).
96. Molinari, N., Mailoa, J. P. & Kozinsky, B. Effect of Salt Concentration on Ion Clustering and Transport in Polymer Solid Electrolytes: A Molecular Dynamics Study of PEO-LiTFSI. *Chemistry of Materials* **30**, 6298–6306 (2018).
97. Mogurampelly, S. & Ganesan, V. Structure and mechanisms underlying ion transport in ternary polymer electrolytes containing ionic liquids. *Journal of Chemical Physics* **146**, 074902 (2017).
98. Costa, L. T., Sun, B., Jeschull, F. & Brandell, D. Polymer-ionic liquid ternary systems for Li-battery electrolytes: Molecular dynamics studies of LiTFSI in a EMIm-TFSI and PEO blend. *Journal of Chemical Physics* **143**, 024904 (2015).
99. Wang, J., Wolf, R. M., Caldwell, J. W., Kollman, P. A. & Case, D. A. Development and testing of a general amber force field. *Journal of Computational Chemistry* **25**, 1157–1174 (2004).
100. Sprenger, K. G., Jaeger, V. W. & Pfaendtner, J. The general AMBER force field (GAFF) can accurately predict thermodynamic and transport properties of many ionic liquids. *Journal of Physical Chemistry B* **119**, 5882–5895 (2015).

101. Molinari, N., Mailoa, J. P. & Kozinsky, B. Effect of Salt Concentration on Ion Clustering and Transport in Polymer Solid Electrolytes: A Molecular Dynamics Study of PEO-LiTFSI. *Chemistry of Materials* **30**, 6298–6306 (2018).
102. Gudla, H., Zhang, C. & Brandell, D. Effects of Solvent Polarity on Li-Ion Diffusion in Polymer Electrolytes: An All-atom Molecular Dynamics Study with Charge Scaling. *The Journal of Physical Chemistry B* **124**, 8124–8131 (2020).
103. Kirby, B. J. & Jungwirth, P. Charge Scaling Manifesto: A Way of Reconciling the Inherently Macroscopic and Microscopic Natures of Molecular Simulations. *Journal of Physical Chemistry Letters* **10**, 7531–7536 (2019).
104. Nymand, T. M. & Linse, P. Molecular dynamics simulations of polarizable water at different boundary conditions. *The Journal of Chemical Physics* **112**, 6386–6395 (2000).
105. Heinz, T. N., van Gunsteren, W. F. & Hünenberger, P. H. Comparison of four methods to compute the dielectric permittivity of liquids from molecular dynamics simulations. *J. Chem. Phys* **115**, 1125 (2001).
106. Newman, J. S. & Balsara, N. P. Electrochemical systems. 577.
107. Onsager, L. Theories and Problems of Liquid Diffusion. *Ann N Y Acad Sci* **46**, 241–265 (1945).
108. Wheeler, D. R. & Newman, J. Molecular dynamics simulations of multicomponent diffusion. 1. equilibrium method. *Journal of Physical Chemistry B* **108**, 18353–18361 (2004).
109. Zhou, Y. & Miller, G. H. Green-Kubo formulas for mutual diffusion coefficients in multicomponent systems. *Journal of Physical Chemistry* **100**, 5516–5524 (1996).
110. Fong, K. D., Bergstrom, H. K., McCloskey, B. D. & Mandadapu, K. K. Transport phenomena in electrolyte solutions: Nonequilibrium thermodynamics and statistical mechanics. *AIChE Journal* **66**, e17091 (2020).
111. Abraham, M. J. *et al.* GROMACS: High performance molecular simulations through multi-level parallelism from laptops to supercomputers. *SoftwareX* **1–2**, 19–25 (2015).
112. Cameron, G. G., Ingram, M. D. & Harvie, J. L. Ion transport in polymer electrolytes. *Faraday Discussions of the Chemical Society* **88**, 55–63 (1989).
113. Lascaud, S. *et al.* Phase Diagrams and Conductivity Behavior of Poly(ethylene oxide)-Molten Salt Rubbery Electrolytes. *Macromolecules* **27**, 7469–7477 (1994).
114. Zheng, Q. *et al.* Optimizing Ion Transport in Polyether-Based Electrolytes for Lithium Batteries. *Macromolecules* **51**, 2847–2858 (2018).

115. Dalvi, A., Parvathala Reddy, N. & Agarwal, S. C. The Meyer-Neldel rule and hopping conduction. *Solid State Communications* **152**, 612–615 (2012).
116. Brooks, D. J., Merinov, B. V., Goddard, W. A., Kozinsky, B. & Mailoa, J. Atomistic Description of Ionic Diffusion in PEO-LiTFSI: Effect of Temperature, Molecular Weight, and Ionic Concentration. *Macromolecules* **51**, 8987–8995 (2018).
117. McDaniel, J. G. & Son, C. Y. Ion Correlation and Collective Dynamics in BMIM/BF4-Based Organic Electrolytes: From Dilute Solutions to the Ionic Liquid Limit. *Journal of Physical Chemistry B* **122**, 7154–7169 (2018).
118. Shen, K. H. & Hall, L. M. Ion Conductivity and Correlations in Model Salt-Doped Polymers: Effects of Interaction Strength and Concentration. *Macromolecules* **53**, 3655–3668 (2020).
119. Woolf, L. A. & Harris, K. R. Velocity correlation coefficients as an expression of particle–particle interactions in (electrolyte) solutions. *Journal of the Chemical Society, Faraday Transactions 1: Physical Chemistry in Condensed Phases* **74**, 933–947 (1978).
120. Fonseca, C. P., Rosa, D. S., Gaboardi, F. & Neves, S. Development of a biodegradable polymer electrolyte for rechargeable batteries. *Journal of Power Sources* **155**, 381–384 (2006).
121. Mindemark, J., Sun, B., Törmä, E. & Brandell, D. High-performance solid polymer electrolytes for lithium batteries operational at ambient temperature. *Journal of Power Sources* **298**, 166–170 (2015).
122. Sun, B. *et al.* Ion transport in polycarbonate based solid polymer electrolytes: experimental and computational investigations. *Physical Chemistry Chemical Physics* **18**, 9504–9513 (2016).
123. Du, J. & Rimsza, J. M. Atomistic computer simulations of water interactions and dissolution of inorganic glasses. *npj Materials Degradation* **1**, 1–12 (2017).
124. Jader, T. B. Molecular Computer Simulations of Graphene oxide intercalated with methanol: Swelling Properties and Interlayer Structure. (Umeå University, 2017).
125. Gudla, H., Shao, Y., Phunnarungsi, S., Brandell, D. & Zhang, C. Importance of the Ion-Pair Lifetime in Polymer Electrolytes. *Journal of Physical Chemistry Letters* **12**, 8460–8464 (2021).

Acta Universitatis Upsaliensis

Digital Comprehensive Summaries of Uppsala Dissertations from the Faculty of Science and Technology 2168

Editor: The Dean of the Faculty of Science and Technology

A doctoral dissertation from the Faculty of Science and Technology, Uppsala University, is usually a summary of a number of papers. A few copies of the complete dissertation are kept at major Swedish research libraries, while the summary alone is distributed internationally through the series Digital Comprehensive Summaries of Uppsala Dissertations from the Faculty of Science and Technology. (Prior to January, 2005, the series was published under the title "Comprehensive Summaries of Uppsala Dissertations from the Faculty of Science and Technology".)

Distribution: publications.uu.se
urn:nbn:se:uu:diva-481109

ACTA
UNIVERSITATIS
UPSALIENSIS
UPPSALA
2022